Bioactive Materials 6 (2021) 2783–2800

Contents lists available at ScienceDirect

Bioactive Materials

journal homepage: www.sciencedirect.com/journal/bioactive-materials

# Multifunctional bioactive core-shell electrospun membrane capable to terminate inflammatory cycle and promote angiogenesis in diabetic wound

Atta ur Rehman Khan [a,1], Kai Huang [b,1], Mina Shahriari Khalaji [c], Fan Yu [a], Xianrui Xie [a], Tonghe Zhu [d], Yosry Morsi [e], Zhao Jinzhong [b,**], Xiumei Mo [a,*]

[a] State Key Laboratory for Modification of Chemical Fibers and Polymer Materials, College of Chemistry, Chemical Engineering and Biotechnology, Donghua University, Shanghai, 201620, PR China

[b] Department of Sports Medicine, Department of Orthopedics, Shanghai Jiao Tong University Affiliated Sixth People's Hospital, No. 600 Yishan Road, Shanghai, 200233, PR China

[c] Microbiological Engineering and Industrial Biotechnology Group, College of Chemistry, Chemical Engineering and Biotechnology, Donghua University, Shanghai, 201620, PR China

[d] Multidisciplinary Centre for Advanced Materials of Shanghai University of Engineering Science, College of Chemistry and Chemical Engineering, Shanghai University of Engineering Science, No. 333 Longteng Road, Shanghai, 201620, PR China

[e] Faculty of Engineering and Industrial Sciences, Swinburne University of Technology, Boroondara, VIC, 3122, Australia

ARTICLE INFO

*Keywords:*
Bioactive NF membrane
Diabetic wound healing
Antibacterial
Antioxidant
Anti-inflammatory
Angiogenesis

ABSTRACT

Diabetic wound (DW) healing is a major clinical challenge due to multifactorial complications leading to prolonged inflammation. Electrospun nanofibrous (NF) membranes, due to special structural features, are promising biomaterials capable to promote DW healing through the delivery of active agents in a controlled manner. Herein, we report a multifunctional composite NF membrane loaded with ZnO nanoparticles (NP) and oregano essential oil (OEO), employing a new loading strategy, capable to sustainedly co-deliver bioactive agents. Physicochemical characterization revealed the successful fabrication of loaded nanofibers with strong in vitro anti-bacterial and anti-oxidant activities. Furthermore, in vivo wound healing confirmed the potential of bioactive NF membranes in epithelialization and granulation tissue formation. The angiogenesis was greatly prompted by the bioactive NF membranes through expression of vascular endothelial growth factor (VEGF). Moreover, the proposed NF membrane successfully terminated the inflammatory cycle by downregulating the pro-inflammatory cytokines interleukin −6 (IL-6) and matrix metalloproteinases-9 (MMP-9). In vitro and in vivo studies revealed the proposed NF membrane is a promising dressing material for the healing of DW.

## 1. Introduction

Diabetes mellitus is one of the major public health concerns owing to its association with the increasing level of mortality and morbidity. About 700 million people are anticipated to be diabetic by 2045 [1]. A major chunk of it is prone to develop diabetic wounds (DW) including diabetic foot ulcers (DFU). A DW remains at high risk of conversion into a chronic non-healing wound due to multiple factors such as metabolic and physiological stresses, hypoxia, neuropathy, ischemia, and infection. A DW is often trapped in a vicious inflammatory cycle due to impaired response to growth factors, poor blood circulation, the persistent release of proinflammatory cytokines, overproduction of reactive oxygen species (ROS), and other microvascular complications [2]. Unlike a normal wound, a DW requires proper treatment to terminate the inflammatory cycle and resume the normal healing process. Simple wound care may not be effective in the diabetic-related wound. Since the complication of DW is multifactorial, specific interventions at various healing phases are required.

Pressure offloading, sharp tissue debridement, management of infection, and surgical resumption of blood circulation are some of the clinical approaches adopted for the management of DW related complications. But the success rate is either limited or varies from person to

Peer review under responsibility of KeAi Communications Co., Ltd.

* Corresponding author.
** Corresponding author.
*E-mail addresses:* jzzhao@sjtu.edu.cn (Z. Jinzhong), xmm@dhu.edu.cn (X. Mo).

[1] These authors contributed equally to this work.

https://doi.org/10.1016/j.bioactmat.2021.01.040
Received 2 October 2020; Received in revised form 25 January 2021; Accepted 31 January 2021

person and also not cost-effective. Many therapies based on growth factors [3–5], protein formulations such as substance P [6], erythropoietin [7], insulin [8], and natural products have been tried but their delivery and bioavailability on wound site require a proper vehicle. Traditional wound dressings only play a protective and passive role. With the advancement of technology, many active wound dressings have been built, able to deliver bioactive substances, such as foams, films, and hydrogels. Simple delivery of active substances may not be beneficial to a maximum extent, a dressing mimicking extracellular matrix (ECM) which could act as a scaffold along with a drug carrier may be more suitable for DW management.

Electrospinning is an old technique but has got great attention in the last decade due to its potential to fabricate nano-size fibers making ECM-like networks capable to deliver bioactive substances as well as guide and promote cell migration and differentiation. Moreover, the ability to exchange gases and absorbing wound exudates make the electrospun NF membrane an ideal scaffold. Considering the potential of electrospun NF, as a promising scaffold material, many researchers attempted to utilize this technology to fabricate biomaterials for DW. Recently, many researchers loaded the nanofibers with various therapeutic agents such as an antibiotic, antioxidants, anti-inflammatory, growth factors, stem cells, and other natural and synthetic compounds and have got the success of varying degrees [9–22]. In all the reported work, a uniaxial approach was opted to treat the multifactorial DW. Only clearing the wound area, from microbial invasion, may not trigger the regeneration process because the infection is not the only cause of prolonged inflammation. On the other hand, the open wound can be prone to develop infection and the formation of biofilm. Angiogenesis is another key factor which ensures the new blood vessel formation making possible the supply of oxygen and nutrient required for regeneration. This is another factor that is adversely affected by diabetic patients due to hyperglycemia directly affecting endothelial cells. Recently, many attempts have been made to trigger angiogenesis through the delivery of iron chelating agents [18,23,24] and successfully promoted the angiogenesis but these fabrications did not possess any antibacterial activity. Moreover, these agents are highly unstable and also pose a risk of adverse effects such as developing tumors. Promoting angiogenesis in DW remains a major challenge.

Zinc oxide is among those metallic oxides which has a substantive role in the wound healing process. Along with direct therapeutic applications such as anti-bacterial, anti-inflammatory activities, it also acts as a micronutrient, highly relevant to the healing process. Moreover, it acts as a co-factor for encoding about 10% of body proteins which play an immense regulatory role such as transcriptional regulations, DNA repair, and ECM construction. More importantly, zinc plays the role in all phases of wound healing including homeostatic, inflammatory, proliferative, and remodeling. The capability of zinc in promoting vascularization, re-epithelialization, and regulation of metalloproteinases (MMPs) makes it highly significant in mitigating DW related complications [25]. Given the highly specific role of zinc oxide in DW, an attempt was made to deliver zinc oxide to the wound site via electrospun nanofiber [26]. According to the outcome, 2% was the optimum concentration effectively promoting angiogenesis and a higher concentration was toxic to the tissues. But 2% of zinc oxide concentration cannot provide the required antibacterial effect. Moreover, the major mechanism of zinc oxide to fight against infection is the production of ROS. In DW wounds, the elevated level of ROS is a major contributor to prolonged inflammation. The co-delivery of another antibacterial agent, with additional antioxidant potential, may provide complete protection against infection but also helps in keeping the balance between ROS production and destruction.

Microbial infection acts as a major cause of delayed DW healing [27]. The systemic use of antibiotics has a limited role in eradicating skin infection. Moreover, the long-term systemic use of antibiotics may result in other complications such as damage to the microflora ecosystem in the digestive tract [28]. The topical delivery of antibiotics can be more effective in combating skin infection. However, the use of a conventional antibiotic may lead to bacterial resistance. The use of natural antibacterial compounds is highly desirable due to increasing bacterial resistance associated with the conventional use of antibiotics. Essential oils are alternative broad-spectrum antimicrobial agents also accompanied by other therapeutic attributes such as anti-inflammatory and anti-oxidant activities. Oregano essential oil (OEO) is a natural plant extract with proven anti-oxidant and anti-bacterial potentials [29,30]. Moreover, we have recently reported the wound healing potential of OEO due to its strong antibacterial and antioxidant activity [30].

Considering the antibacterial, anti-inflammatory, and antioxidant potential of these two above mentioned bioactive agents, we developed a hypothesis that an intervention in the inflammatory phase of DW through co-delivery of ZnO and OEO may help accelerate the healing process by the anti-inflammatory action of ZnO and OEO. The radical scavenging potential of OEO may help in the formation of a temporary ECM network for granulation. Moreover, neo-vascularization is highly anticipated which ensures the supply of oxygen and nutrients to newly forming tissues.

We have chosen the electrospinning technique for the dual loading of bioactive agents (ZnO and OEO). Poly (L-lactide-co-caprolactone) (PLCL) is a synthetic polymer with excellent mechanical properties, biocompatibility as well as biodegradability [31]. Moreover, its potential as a drug carrier is also evident [32,33]. But its poor wettability makes it slightly disadvantageous as a dressing material. Hyaluronic acid is a polymer naturally present in the ECM network [34]. The presence of hyaluronic acid can not only resolve the wettability issue but also signal cellular proliferation and migration [35,36]. Electrospinning provides flexible options to load bioactive compounds through blending, chemical, and physical immobilization, co-axial, and emulsion spinning. Co-axial spinning is a widely used method for the sustained delivery of bioactive substances. Moreover, co-axial electrospinning is also suitable for dual drug loading separated by core and shell. Co-axial electrospinning can be very helpful in loading volatile compounds in the core for stable loading. Till now, many electrospinning techniques have been employed to encapsulate the essential oils such as blending, emulsion, and co-axial spinning. Both emulsion and co-axial spinning provide a shell layer to protect volatile compounds but still, controlled delivery is a challenge.

We used a modified technique of loading OEO. We developed an oil in water emulsion, stabilized by a surfactant tween 80, and loaded it into the core during electrospinning via a core nozzle. We are introducing a modified loading technique. The basic aim of this modification is to provide an extra layer to encapsulate OEO. Whereas, ZnO NP were blended with PLCL to form a shell layer. The detailed fabricating process is illustrated in Fig. 1A.

The basic aim of the study is to make possible the sustained co-delivery of two bioactive agents and to analyze how their synergistic action may be beneficial in DW healing in terms of antibacterial, antioxidant, anti-inflammatory activities. Four different types of NF membranes named PLCL, PLCL/Z, PLCL/E, and PLCL/Z/E were fabricated followed by detailed physicochemical and biological evaluation (Fig. 1B).

## 2. Materials and method

### 2.1. Materials

The copolymer of poly (L-lactide-co-caprolactone) (PLCL) (50:50) was purchased from Jinan Daigang Biomaterials Co., Ltd (China) and 1,1,1,3,3, 3, -hexafluoro-2-isopropanol (HFIP) from Daikin Industries Ltd (Japan). Hyaluronic acid ($M_W$ = 100,00–20000 Da) was sourced from Liuzhou Shengqiang Biotech Co., Ltd, Guangxi, China, and ZnO nanoparticle (size $\leq$ 40 nm) from Sigma-Aldrich 3050 Spruce, St. Louis, MO 63103, USA. Oregano Essential Oil (OEO) (100% pure) extracted from *Origanum vulgare,* through steam distillation (Edens Garden, 1322

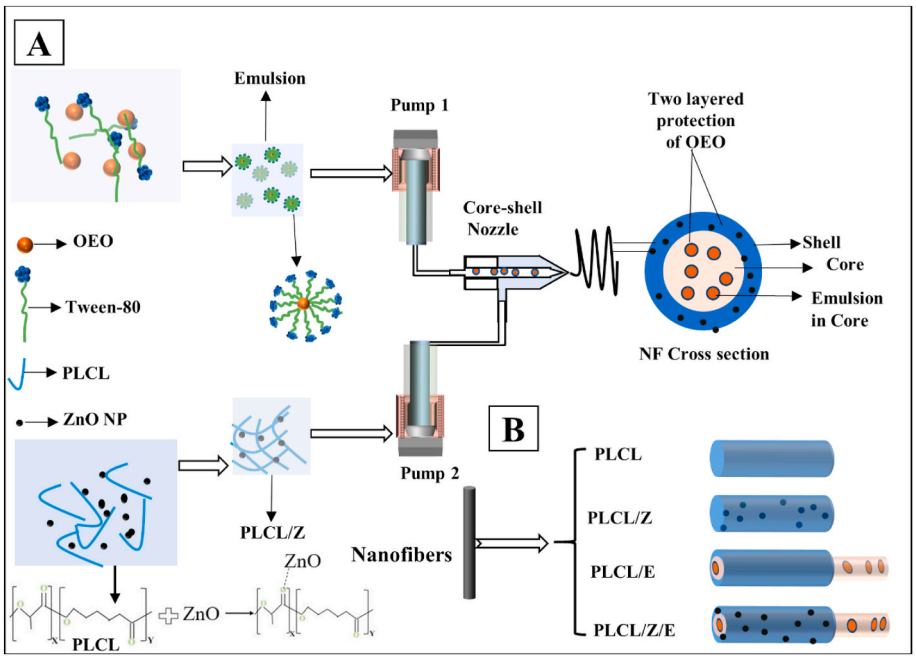


**Fig. 1.** Schematic illustration of fabrication mechanism of a nanofibrous membrane (A) representative image showing the formation of oil in water emulsion, the interaction between PLCL and ZnO NP followed by fabrication of core-shell nanofiber encapsulating ZnO NP and oil emulsion, (B) Four types of nanofibers fabricated for analysis.

Calle Avanzado, San Clemente, CA 92673, USA). Cell counting Kit-8 (CCK-8) 2-(2-methoxy-4-nitrophenyl)-3-(4-Nitphenyl)-5-(2,4-disulfophenyl)-2H-tetrazolemonosodium salt) and Phosphate-buffered saline (PBS) (pH 7.2–7.4) were procured from Beijing Solarbio Science & Technology Co., Ltd, China. Cell culture media including Dulbecco's Modified Eagle's Medium (DMEM) High Glucose (1640), Fetal Bovine Serum (FBS), and related media reagents were obtained from Gibco Life Technologies, Co. Waltham, Massachusetts, USA. Bacterial Culture Media (LB Broth, LB Broth Agar) was purchased from Sangon Biotech (Shanghai) Co., Ltd, China. Bacterial live/dead staining dye, *Bac*Light, was purchased from Thermo Fisher Scientific, Shanghai, China. L Ascorbic Acid (AA) was gotten from Sinopharm Chemical Reagent Co., Ltd, China whereas, 2,2-diphenyl-1-picryl-hydrazyl-hydrate (DPPH) was acquired from Alfa Aesar chemical co., Ltd, China.

## 3. Fabrication of nanofibers

### 3.1. Preparation of oil emulsion and spinning solutions

Oil emulsion was prepared by adding 10% OEO in drops into 2% hyaluronic acid (HA) solution and complete dispersion was achieved through constant stirring for 1h at room temperature. Furthermore, 2% v/v tween 80 surfactants were added to the OEO/HA solution followed by stirring to make oil in water emulsion. To minimize the droplet size, the crude emulsion was sonicated using a 25 kHz ultrasonic homogenizer for 20 min. All the concentrations were selected based on preliminary emulsification tests. Emulsion (E) was used as a core solution.

For making shell solutions, PLCL 8% (w/v) was dissolved in HFIP and kept on stirring overnight under room temperature, and 2% w/v zinc oxide nanoparticles (ZnO NP) were added into PLCL solution followed by sonication for complete dispersion. Two different solutions were prepared; PLCL only and PLCL having ZnO NP (PLCL/Z).

### 3.2. Electrospinning

Four different types of nanofibrous (NF) membranes were fabricated named PLCL, PLCL/Z, PLCL/E, and PLCL/Z/E. The basic electrospinning apparatus used for the fabrication consisted of syringe pumps (789100C, Cole-Parmer Instrument, USA), a metal plate collector, and a high-voltage power supply (BGG6-358, BMEI Co Ltd, Beijing China). For making PLCL and PLCL/Z nanofibers, 10 mL of each solution was placed in a plastic syringe with a 21 Gauge needle. The syringe was loaded onto the pump and the flow rate was kept at 1.2 mL/h. Whereas, the distance between the metal plate collector and syringe was maintained between 12 and 14 cm and voltage at 10 kV. Moreover, humidity and temperature were also kept constant at 50% and 25 °C respectively throughout the spinning process. Whereas, core-shell nanofibers named PLCL/E and PLCL/Z/E were fabricated using a core-shell nozzle connected with two separate pumps. The flow rate for the shell solution was kept at 1 mL/h, whereas, the core solution's flow rate was 0.1 mL. Other spinning parameters were the same as described above. After the fabrication, the NF membranes were kept in a vacuum dryer for 3 days under the temperature of 25 °C before further characterization and evaluation.

## 4. Characterization

### 4.1. Physicochemical characterization

The surface morphology and the elemental mapping of the NF membrane were studied by scanning electron microscopy (SEM, Hitachi, TM-1000, Japan) with an EDX spectrometer after gold coating (10 mA, 45 s). To calculate the average fiber diameters, the hundred randomly selected nanofibers, from SEM images, were analyzed using Image J software (National Institutes of Health, USA). The core-shell structure and the presence of ZnO NP within a single nanofiber were observed by transmission electron microscopy (TEM, JEM-2100, JEOL, Japan). To collect the sample for TEM, carbon-coated Cu grids were placed near the collector for the deposition of a single nanofiber. To confirm the loading of ZnO and oil emulsion and their possible impact on the crystallinity of NF membranes, we used XRD. XRD was recorded in the $2\theta$ range of 10°–80° using a model D8 ADVANCE from Bruker (Germany) with CuKα radiation of 8.04 keV and wavelength of 1.54 Å. The applied voltage and the current were 40 kV and 25 mA respectively.

The surface hydrophilicity of NF membranes was studied by

measuring the water contact angle (WCA) using a contact angle measurement instrument (DSA30, Kruss, Germany).

The release of ZnO NP was determined by inductively coupled plasma atomic emission spectrometer (ICP-AES, Perkin-Elmer Optima 20 0 0, USA). The release medium consisted of PBS and about 20 mg of sample was weighed and put in 4 mL of PBS. At different time points, 2 mL of medium was withdrawn and replaced by a fresh one. The collected samples were stored at −20 °C till Zn ion release determination.

OEO is a complex mixture of more than 50 components but carvacrol is the major component constituting more than 80% according to gas chromatography-mass spectrometry (GCMS) report of utilized OEO [37]. Therefore, we selected carvacrol to determine the oil release profile. The release of carvacrol from the emulsion and nanofiber core was studied through liquid chromatography-mass spectrometry (LCMS) following the procedure of our previous work [29]. Briefly, 20 mg membrane was taken and immersed in 2 mL of PBS. 1 mL of PBS was withdrawn at a predefined time point and replaced with a fresh one. The samples were stored at −20 °C till the release determination.

The mechanical properties of the PLCL, PLCL/Z, PLCL/E, and PLCL/Z/E were characterized by the Universal Materials Testing Machine (H5K–S, Hounsfield, UK) with an ambient temperature of 20 °C and humidity of 65%. All specimens (50 mm × 10 mm, n = 5) were tested with a cross-head speed of 10 mm $min^{-1}$ until breakage. Before testing, specimen thickness was measured using a digital gauge meter, having a precision of 1 μm.

## 5. Biological evaluation

### 5.1. Determination of minimum inhibitory concentrations (MIC)

The liquid dilution method was opted to find the MIC of both ZnO NP and OEO following the previously described method [38]. Briefly, both *S. aureus* and *E. coli* were precultured in Broth culture media overnight and culture containing ($10^8$ CFU/mL cells). Initially, 6 mg ZnO NP were dissolved in 2 mL Broth culture media, and subsequently, two folds dilutions were achieved. Whereas, 1000 μl OEO was dissolved in 2 mL Broth media, and 1% tween 80 was also added to facilitate the oil dilution. Also, two-fold dilutions were achieved. 100 μl bacterial culture was added to 900 μl culture media having various concentrations of ZnO and OEO. The turbidity was measured after incubating for 24 h. The lowest concentration with invisible turbidity was considered MIC for both antibacterial agents.

### 5.2. Antibacterial activity

Antibacterial efficacy (%) was quantified using the turbidity measurement method. PLCL, PLCL/Z, PLCL/E, and PLCL/Z/E NF membranes were cut (50 mg weight) and sterilized under UV light for 4 h before antibacterial testing. LB broth liquid culture media was prepared to culture both *E. coli* (BCRC 11634) and *S. aureus* (BCRC 10451) strains using the manufacturer's protocol. A single colony of both strains was transferred to a liquid medium under sterile conditions and kept in an incubator at 37 °C in shaking mode (100 rpm) for 24 h. The media was diluted to get a final optical density (OD) of 0.5. A set of six test tubes were taken for each strain, labeled as A-F, and 5 mL of culture media was added to each tube. Tube A was taken as blank (only culture media). 100 μl bacterial culture (both strains) was added in tube B–F. Tube B was taken as control (only bacterial culture). Whereas, PLCL, PLCL/Z, PLCL/E, and PLCL/Z/E NF membranes were put in tubes C, D, E, and F respectively. All these tubes were kept in an incubator at 37 °C under shaking conditions for 24 h. After 24 h, OD was measured at 600 nm, and the antibacterial activity of each NF membrane was calculated. Before calculating the antibacterial activity, OD was corrected by subtracting the OD of blank culture media. Since the OD of bacterial culture remains proportional to the number of bacteria, antibacterial activity (%) can be calculated using the equation (i).

$$\text{Antibacterial activity } (\%) = (Ic\text{-}Is)/Ic \times 100 \quad \text{(i)}$$

Where *Ic* is the OD of the control group and *Is* is the OD of the experimental group.

The images were also taken, after 24 h, to observe the change in turbidity of culture media in various experimental groups.

To observe the microbiocidal effect of the nanofibers, a set of four Petri dishes were prepared using solid culture media. About 200 μl sample from tube C–F was taken and spread gently on the surface of culture media. The Petri dishes were kept in an incubator in an inverted position for 24 h. After 24 h, the images were taken to observe the colonies on the surface.

The viability of bacteria, seeded on the scaffolds, was also examined using a fluorescence microscope. After culturing for 24 h, bacteria-seeded scaffolds were washed with distilled water and treated with propidium iodide (2 μl) and SYTO ® 9 (2 μl) (Live/Dead Viability Kit) in each well for 15 min at room temperature. Bacteria were observed and photographed using fluorescence microscope.

To observe the growth of bacteria, both strains were cultured on the surface of NF membranes in 24 well plates. Briefly, 14 mm disc-shaped NF membranes were cut and placed in 24 well plates. 1 mL pre-culture of bacteria, having OD value 0.5, was poured in each well and put in an incubator at 37 °C for 24 h. After 24 h, the culture media was removed and NF membranes were gently washed with PBS. Afterward, cells were fixed using 4% (v/v) paraformaldehyde solution for 4 h at 4 °C. The NF membranes were dehydrated with different ethanol concentrations of 30, 50, 70, 90, and 100% (v/v) respectively before being dried. Subsequently, samples were gold coated for 45 s. The SEM images were taken at an accelerating voltage of 15 kV to observe the morphology of bacteria grown on different designated NF membranes.

### 5.3. Antioxidant activity

2,2-diphenyl-1-picryl-hydrazyl-hydrate (DPPH) assay was employed to determine antioxidant activity according to the prescribed method. 0.3 mM of DPPH radical solution was prepared, and samples including PLCL, PLCL/Z, PLCL/E, and PLCL/Z/E (10 mg weight each) and ascorbic acid (AA) were mixed and kept in the dark at room temperature for 30 min. Pure AA was taken as a standard antioxidant agent. Whereas, DPPH solution without NF membranes was taken as blank. The antioxidant activity (%) was calculated using equation (ii).

$$\%\ \text{DPPH Scavenging Activity} = (A_B\text{-}A_S)/A_B \times 100 \quad \text{(ii)}$$

Whereas $A_B$ is the absorption of the blank and $A_S$ is the absorption of the experimental samples (NF membranes). Images of DPPH solutions after 30 min were also taken to observe color changes due to the radical scavenging by various experimental specimens.

### 5.4. In vitro cell culture

NIH-3T3 cells were cultured in Dulbecco's modified eagle's medium (DMEM) containing 10% fetal bovine serum (FBS) and 1% antibiotic-antifungal agent in an atmosphere of 5% $CO_2$ and 37 °C, and the medium was changed every other day. All samples of NF membranes were placed in 24-well plates and fixed with stainless steel rings. Before cell seeding, the NF membranes were sterilized under UV light for 12 h followed by washing with PBS 3 times, and then incubated with high glucose medium for 2h. NIH-3T3 cells were cultured at a density of 20,000 cells/Wells.

The CCK-8 method and calcein-AM and propidium iodide (live/dead) fluorescent staining were used to evaluate the viability of the proliferated NIH-3T3 cells cultured on different NF membranes (n = 3 per group). The NIH-3T3 cultured on the scaffolds for 1, 4, and 7 days in medium, cell-seeded scaffolds were washed thrice with PBS. Then, cells were incubated in 10% (v/v) CCK-8 in DMEM at 37 °C for 1.5h in

standard culture conditions. The supernatant was collected and transferred into a 96 well plate. The fluorescence of the supernatant was measured using a microplate reader (Multiskan MK3, Thermo) at an excitation wavelength of 450 nm. The experiment was repeated thrice for each group.

The viability of NIH-3T3, seeded on the scaffolds, was also examined using a fluorescence microscope. After culturing for 4 days, cell-seeded scaffolds were washed with PBS three-time and treated with propidium iodide (PI, 0.5 μM) and Calcein AM (0.25 μM) (Live/Dead Viability Kit) for 15 min at room temperature. Cells were observed and photographed under an inverted fluorescence microscope (IX53, Olympus).

Besides, the morphology of NIH-3T3 seeded on the scaffolds was visualized using a confocal laser scanning microscope (CLSM, Carl Zeiss LSM 700, Germany). After the 4th and 7th days of culture, the NIH-3T3 were fixed in 4% paraformaldehyde and permeabilized with 0.1% Triton X-100 for 5 min, followed by incubated with 1% bovine serum albumin (BSA). Then, the cells were treated with Alexa Fluor@568 phalloidin (F-actin) (green, stain the cytoskeleton) and 4′,6-diamidino-2-phenylindole (DAPI) (blue, stain the nucleus) for 30 min and 10 min at room temperature respectively. Subsequently, the images were acquired by CLSM. Besides, the morphology and adhesion of cultured cells were also observed through SEM images after culturing for 4 and 7 days.

### 5.5. In vivo experiments

Male Sprague Dawley rats weigh between 200 g–300 g were used to assess the potential of NF membranes in wound healing. The animal experiments were conducted following the protocol approved by the animal experiment ethics committee of Shanghai sixth people's hospital, Shanghai, China.

### 5.6. Induction of a diabetic animal wound model

A large dose of streptozocin (STZ) can directly cause extensive destruction of islet beta cells, which can create a diabetes mellitus model [39]. The diabetic wound model was created using the protocol described by Zhang et al. [40]. Briefly, STZ was dissolved in 0.1 M citrate buffer (pH 4.5) at the concentration of 1G/mL, and the STZ was injected according to the fasting body weight. The injection was completed within 5 min after preparation of STZ solution. The STZ is easy to be inactivated. The solution was covered by aluminium foil paper to avoid light.

Male Sprague Dawley rats (200 g–300 g) were selected. After fasting for 12h, STZ solution (60 mg/kg) was injected intraperitoneally. The diabetic wound model was confirmed by monitoring the fasting glucose level (FGL). The FGL was elevated to an average level of 27 mmol/L after 1–2 weeks of STZ injection. The rats were anesthetized with 0.5% Pentobarbital Sodium at 0.9 mL/100 g body weight. A circular wound, with a diameter of 18 mm, was created on the dorsal side of the rats and fixed with a stainless-steel ring (diameter of 18 mm). In the experimental group, the electrospun NF membrane was fixed under the stainless-steel ring through suture. The wound surface was covered with gauze to prevent contamination from entering the wound. The animals were killed on the 5th, 10th, and 15th days. The wound was evaluated and photographed using a digital camera (Lumix FS16, Panasonic ® Japan) on Days, 05, 10, and 15. The wound area was calculated using ImageJ (NIH) software and the wound closure rate (%) was calculated using equation (iii).

$$\text{Wound closure } (\%) = [(A_0\text{-}A_t)/A_0] \times 100 \quad \text{(iii)}$$

Where $A_0$ is the initial wound area and $A_t$ is the wound area at different time points Three rats were used in each group at different time points.

A full-thickness skin sample was taken from the wound. The tissue samples were immediately fixed in 10% paraformaldehyde solution at room temperature for 48 h. After fixation, the samples were stored at -80 °C until used for further analysis.

### 5.7. Histological staining

For histology analysis, the rats were sacrificed after 5, 10, and 15 days, and tissues were obtained from the wound bed as well as surrounding healthy skin. The specimens were fixed using 4% paraformaldehyde, dehydrated with a series of ethanol (from 30% to 100%), and dimethyl benzene followed by immersion in paraffin. 5 μm sections of skin tissue were cut, deparaffinized and rehydrated followed by staining with hematoxylin-eosin (H&E) to visualize various histology changes such as re-epithelialization and granulation tissue formation. Moreover, tissues were also stained by Masson's trichrome to observe the collagen deposition and neo-vascularization during the healing process. Images were taken using an optical microscope. The largest diameter of the wound bed section was chosen to take images having both left and right sides as normal skin for comparison.

### 5.8. Immunohistochemical analysis

Immunohistochemical staining of vascular endothelial growth factor (VEGF) was performed on days 10 and 15. The deparaffinized and rehydrated tissue sections were incubated with 3% $H_2O_2$ for 10 min. To recover the antigen, slides were put into citric acid antigen repair buffer (pH 6.0) and heated in a microwave oven twice for 8 and 7 min respectively. For blocking endogenous peroxidases, the slices were put into a 3% $H_2O_2$ solution in dark for 25 min. For serum blocking, 3% BSA was added and sealed at room temperature for 30 min. The first antibody, anti-VEGF, was put and incubated overnight at 4 °C. The rabbit anti-VEGF primary antibody (1: 200, Abcam) was incubated with the tissue at 4 °C overnight. The second antibody, HRP goat antirabbit, was kept at room temperature for 50 min. The antibody binding sites were visualized by incubation with a 3,3′-Diaminobenzidine (DAB)/$H_2O_2$ solution. The slides were counterstained for 1 min with hematoxylin and then dehydrated through sequential ethanol before sealing. All slides were observed with a CIC xsp-c204 fluorescence microscope.

### 5.9. Fluorescence quantitative polymerase chain reaction (FQ-PCR)

PCR was employed to study the expression of IL-6 and MMP-9 following the previously described protocol [40]. Briefly, about 100 mg of tissue was completely homogenized before RNA extraction using RNA extract (Wuhan Seville Biotechnology Co., Ltd. g3013). Nanodrop 2000 was used to detect the concentration and purity of RNA. After the instrument was blankly adjusted to zero, 2.5 μL of RNA solution to be tested was put on the detection base, the sample arm was put down, and the software on the computer was used to detect the absorbance value. The final concentration of RNA was 200 ng/μL. The purified extract was further processed using FQ- PCR instrument ABI 7300. After the total RNA was extracted, reverse transcription was done at 95 °C for 10 min (40 cycles, 15s–60s) with reverse transcriptase and primer. The Glyceraldehyde-3-phosphate dehydrogenase (GAPDH) was used as a housekeeping gene as a control. The primer sequence, designed by the PCR primer design tool primer 3, used for PCR is shown in Table 1.

**Table 1**
Primer sequence used for fluorescent quantitative PCR.

| Primers name | Primer sequence |
|---|---|
| R-IL-6-(rz)-F | AATGAGAAAAGAGTTGTGCAATGG |
| R-IL-6-(rz)-R | AGGTAGAAACGGAACTCCAGAAGA |
| R-MMP9-S | GCAAACCCTGCGTATTTCCATT |
| R-MMP9-A | GCGATAACCATCCGAGCGAC |
| R-GAPDH-S | CTGGAGAAACCTGCCAAGTATG |
| R-GAPDH-A | GGTGGAAGAATGGGAGTTGCT |

### 5.10. Statistical analysis

All the experiments were performed in three independent studies and quantitative data were expressed as a mean ± standard deviation (SD). The statistical analysis was carried out using one-way analysis of variance (ANOVA) followed by Tukey's multiple comparison test (n = 3 except mechanical test) and a value of $p < 0.05$ was considered statistically significant.

## 6. Results

### 6.1. Fabrication and physicochemical characterization

Fig. 1A is the schematic illustration of the fabrication of the core-shell NF membrane loaded with ZnO NP in the shell and oil emulsion in the core. OEO could successfully be dispersed into a 2% HA solution by vigorous stirring for 1 h. But the emulsion was not stable. To stabilize the emulsion, tween 80 surfactant was used which formed a stable emulsion due to a special hydrophobic tail and a hydrophilic head. This structure resulted in a stable oil in water emulsion. Although this emulsion can be made by simple homogenization, however, the emulsion was undergone sonication to reduce the droplet size. Finally, a stable emulsion with small droplets was achieved. This emulsion was loaded in the core. Whereas, PLCL blended with ZnO NP was passed on through a shell nozzle attached to the power supply. In total, four different types of NF membranes were fabricated named PLCL, PLCL/Z, PLCL/E, and PLCL/Z/E as shown in Fig. 1B. PLCL and PLCL/Z were fabricated using simple electrospinning. Whereas, PLCL/E and PLCL/Z/E were fabricated using co-axial electrospinning.

SEM was employed to study the surface morphology. SEM analysis

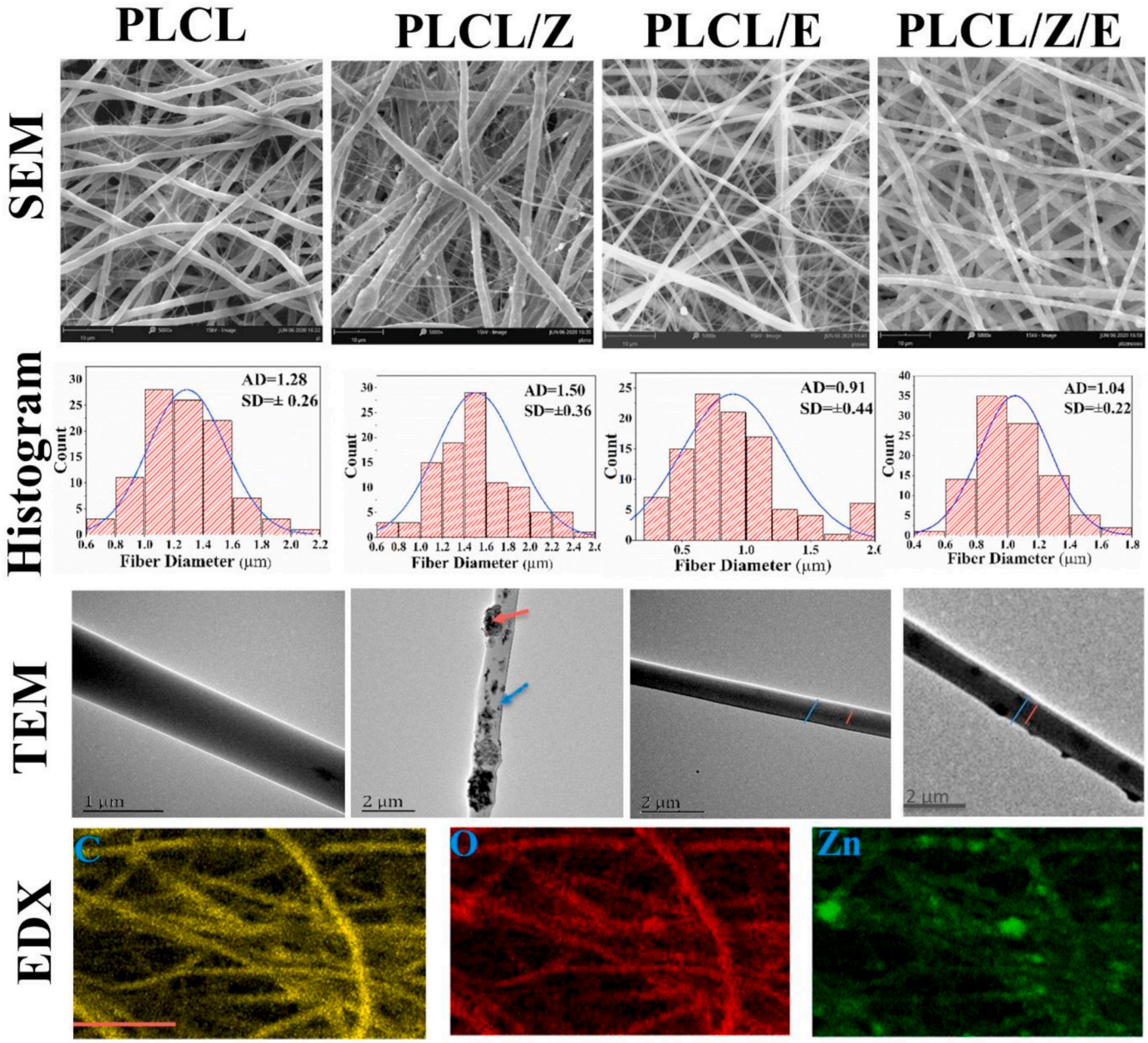


**Fig. 2.** Representative images of PLCL, PLCL/Z, PLCL/E, and PLCL/Z/E showing surface morphology through SEM, histogram exhibiting average fiber diameter with SD±, TEM confirming the loading of ZnO NP in both single-particle (represented by the blue arrow) and aggregation (represented by the orange arrow) and confirming core-shell structure, represented by orange and blue line respectively, in PLCL/E and PLCL/Z/E., and EDX of PLCL/Z indicating the presence of C, O, and Zn. (Scale bar used for EDX = 10 μm).

revealed the web-like structure with a smooth surface. However, the membranes loaded with ZnO NP show some particle aggregation on the surface of fiber which made the surface rougher (Fig. 2). Diameter size distribution showed a statistically significant ($p < 0.05$) difference in fiber diameter among all membranes with PLCL/Z being the highest. PLCL/E NF membrane showed the least fiber diameter among all (Fig. 2). Elemental scanning of the membrane, loaded with ZnO NP, confirmed the even distribution of ZnO NP within the fiber arguing the successful loading through electrospinning (Fig. 2). Internal fiber morphology was studied through TEM. The loading pattern of ZnO NP, revealed from TEM images, depicted the presence of ZnO NP inside the matrix as well as on the surface. The distribution pattern of ZnO NP is both a single particle as well as clusters. The core-shell structure of PLCL/E and PLCL/Z/E was also confirmed through TEM showing successful loading of oil emulsion within the core of the nanofiber (Fig. 2).

XRD pattern of pure HA ZnO NP and electrospun NF membrane is shown in Fig. 3A. According to the XRD pattern, HA turned out to be semi-crystalline displaying a small peak around 28°. Whereas, ZnO NP showed at least five peaks among which peaks around 31°, 34°, and 36° were more prominent. Representative peaks for PLCL were at 16° and 22°. From the XRD pattern, we can confirm the loading of ZnO into PLCL/Z and PLCL/Z/E through peaks marked with steric. Since no new peak appeared in PLCL/Z that confirmed the physical interaction of ZnO and PLCL mainly through H-bonding as shown in Fig. 1. Whereas, the representative peak of PLCL at 22° was more intensified in core-shell membrane loaded with oil emulsion confirming the presence of emulsion. Since no new peak appeared, it indicated that there was no chemical interaction among PLCL, ZnO NP, and emulsion.

The hydrophilicity of the fabricated membrane was assessed by measuring the water contact angle. According to the results, the PLCL membrane showed hydrophobic nature with a contact angle of 121° (Fig. 3B). Which further increased with the addition of ZnO NP. But the difference was statistically insignificant ($p < 0.05$). However, the core-shell membrane having emulsion in the core drastically decreased the water contact angle up to 19° due to the presence of hyaluronic acid in the emulsion. The addition of ZnO in the shell slightly increased the contact angle up to 62° in PLCL/Z/E but still, the membrane was well within the range of hydrophilic limits (Fig. 3B). Inductively coupled plasma atomic emission spectrometry (ICP-AES) was employed to study the release of $Zn^{+2}$ into the release medium. According to the data, the biphasic release of $Zn^{+2}$ from PLCL/Z/E membrane was noted; a burst release of up to 621.2 μg for the initial 6 h followed by sustained release of 311.8 μg for an additional 66 h (Fig. 3C). Total cumulative $Zn^{+2}$ release, up to 72 h, was about 933.07 μg. Whereas, from PLCL/Z, 256.5

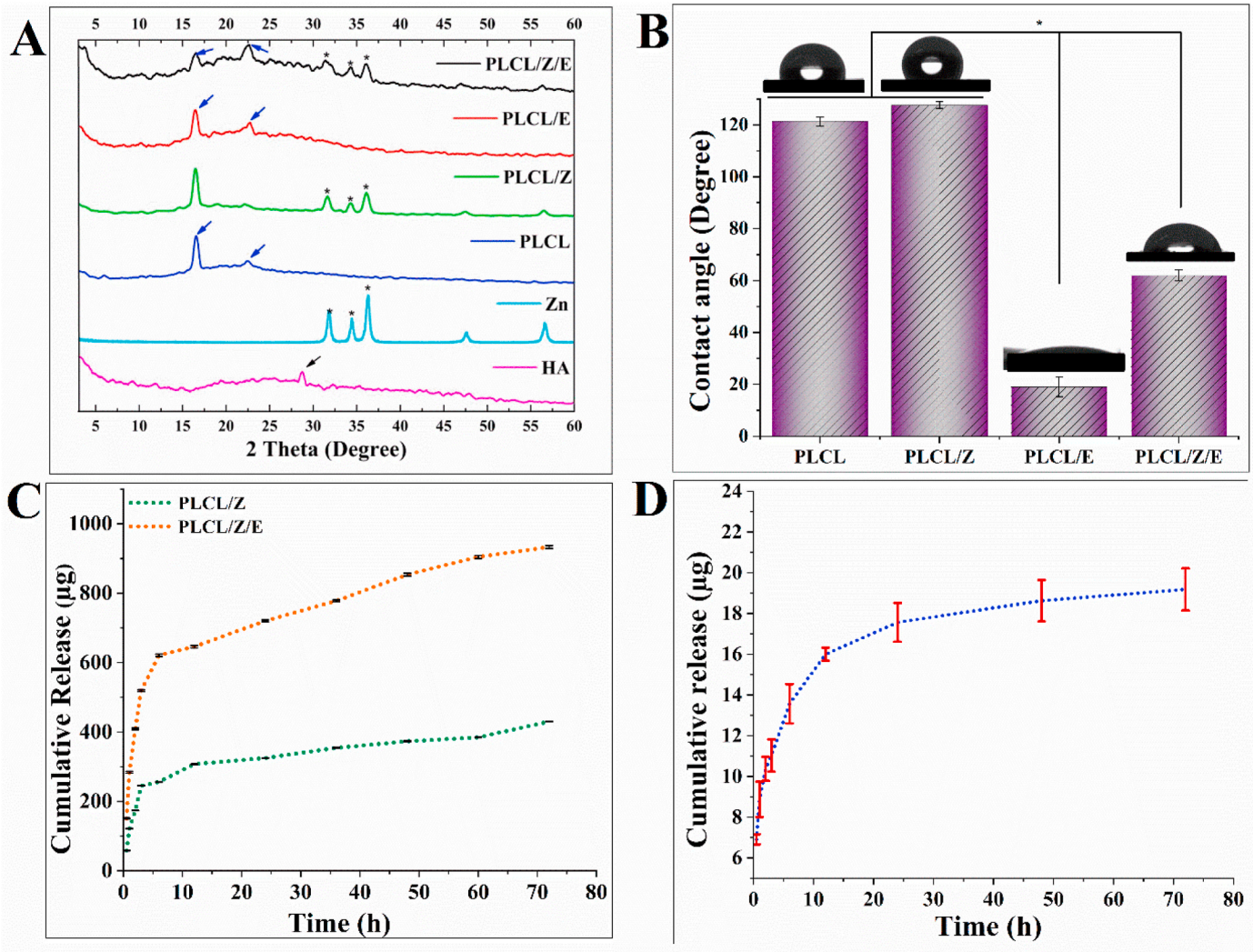


**Fig. 3.** A representative image exhibiting physicochemical characterization of various nanofibrous membranes (A) XRD pattern confirming the successful blending of PLGA and SF and loading of ZnO NP and oil emulsion(B) Water contact angle of the various electrospun membrane, (C) Cumulative release of Zn ion from PLCL/Z and PLCL/Z/E (D) Release of carvacrol form PLCL/Z/E. Statistical analysis was performed by one-way ANOVA followed by Tukey's multiple comparison test, n = 3, *$p < 0.05$.

μg/mL $Zn^{+2}$ release was noted for an initial 6 h followed by a cumulative sustained release up to 430.6 μg for the additional 6 h. A similar pattern was also noted for carvacrol release. A burst release of 16 μL/mL for an initial 12 h followed by sustained release up to 3.18 for the additional 60 h. The total carvacrol release was estimated as 19.18 μL/mL for 72 h (Fig. 3D).

Fig. 4A is the representative image of the typical stress-strain curve and Fig. 4B showing the ultimate tensile strength (MPa) for all NF membranes. From the graphs, it can be deduced that PLCL is a polymer with substantial tensile strength. The ultimate tensile strength of PLCL remained 6.03 MPa which reduced to 4.24 MPa with the addition of ZnO. Whereas, no significant difference was noted in elongation at break as shown in Fig. 4C. However, the young's modulus exhibited a different pattern. According to the results, the modulus for PLCL and PLCL/Z remained insignificantly different ($p < 0.05$) but both were significantly different ($p < 0.05$) from PLCL/E. The highest modulus of 2.61 MPa was noted for PLCL/E (Fig. 4D). These results demonstrated that the addition of 2% ZnO NP affected the tensile strength of the PLCL.

## 7. Biological evaluation

### 7.1. Minimum inhibitory concentration

Mic was determined to find the minimal concentrations of ZnO and OEO capable to inhibit the growth of *S. aureus* and *E. coli*. Table 2 displays the MIC value for both antibacterial agents against two strains of bacteria. According to the result, MIC of ZnO remained 93.75 μg/mL and 46.87 μg/mL against *E. coli* and *S. aureus* respectively. MIC of OEO remained 1.95 μL/mL and 0.98 μL/mL against *E. coli* and *S. aureus* respectively.

**Table 2**
Minimum inhibitory concentrations of ZnO NP and oregano essential oil.

| ZnO (μg/mL) | OEO (μl/mL) |
|---|---|
| ***E. coli*** | 93.75 | 1.95 |
| ***S. aureus*** | 46.87 | 0.98 |

### 7.2. Antibacterial activity

A quantitative method was employed to determine the antibacterial activity of the fabricated membranes. Two model strains of bacteria *E. coli* and *S. aureus* were used to assess the antibacterial potential against both gram-positive and gram-negative bacteria. The antibacterial activity of PLCL was almost negligible. Whereas, antibacterial activity of PLCL/Z, PLCL/E, and PLCL/Z/E against *E. coli* remained 55, 49, and 99% respectively. Whereas, the antibacterial activity of the same NF membranes remained 61, 48, and 98% respectively (Fig. 5A). These results indicated that both ZnO NP and OEO were antibacterial and their co-delivery demonstrated a synergistic action making the antibacterial

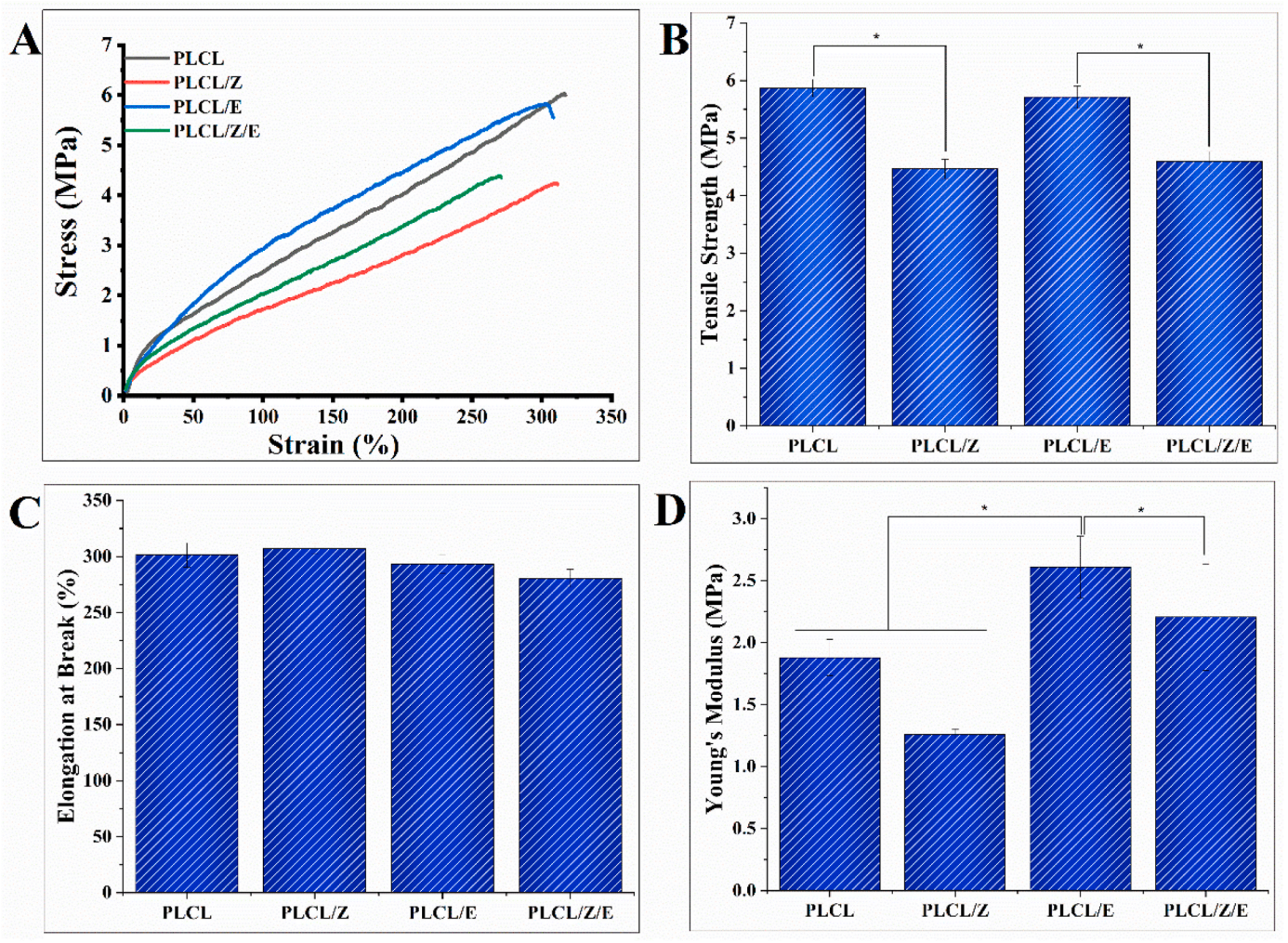


**Fig. 4.** The image representing the mechanical properties of various nanofibrous membranes (A) typical stress-strain curve, (B) ultimate tensile strength, (C) elongation at break, (D) Young's modulus. Statistical analysis was performed by one-way ANOVA followed by Tukey's multiple comparison test, n = 5, $*p < 0.05$.

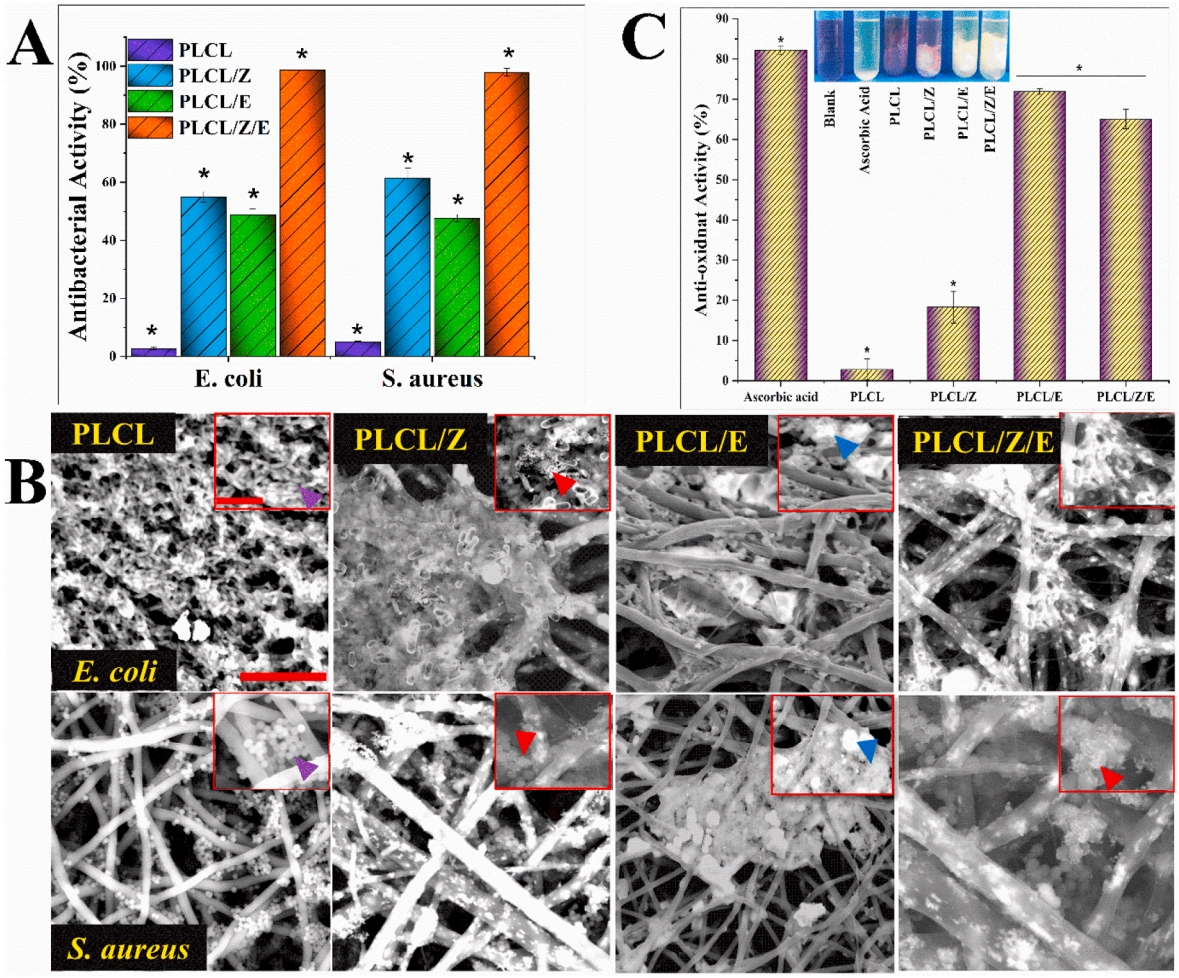


**Fig. 5.** Representative graph showing antibacterial and antioxidant activities of various NF membranes (A) Graph exhibiting the antibacterial activity against *E.coli* and *S. aureus* measured through turbidity method (B) SEM image showing the growth of bacteria on the surface of various NF membrane. Intact bacterial cells and deformed colonies are indicated by the purple and blue arrowhead. Red arrowheads indicate the attachment of ZnO NP on the surface of the bacterial cell (scale bar = 10 μm, mag scale bar = 5 μm) (C) representative graph of antioxidant activity (%) and image of color changes due to scavenging activity measured through DPPH radical scavenging assay. Statistical analysis was performed by one-way ANOVA followed by Tukey's multiple comparison test, n = 3, $*p < 0.05$.

potential stronger. Fig. S1 (A-F) is the representative image of various tubes showing turbidity which was proportional to the growth of bacteria. Whereas, culture media without bacteria displayed no turbidity. The turbidity in tube B and C (*E. coli* and *S. aureus*)) was similar concluding that PLCL did not retard bacterial growth. In contrast, turbidity significantly decreased in tubes D and E which was related to a reduced number of bacterial growths. Moreover, tube E had displayed no turbidity indicating the complete absence of bacteria (Fig. S1). These results demonstrated the synergy between ZnO NP and OEO against bacteria.

To demonstrate the microbiocidal effect of ZnO, OEO, and their combination, we took about 200 μm of bacterial culture from designated tubes (C–F) and spread on petri dishes containing solid culture media. Fig. S2 is the representative image showing the number of colonies grown on solid culture media. The results also indicate the correlation between the presence, absence, and co-presence of ZnO NP and OEO in NF membranes and the number of bacterial colonies. The media withdrew from tube C, having PLCL membrane, showed the maximum colony growth for both the strains. Whereas, bacterial colonies drastically decreased for PLCL/Z and PLCL/E. However, the presence of a few colonies indicated that 100% antibacterial activity cannot be achieved in these concentrations. However, the co-presence of both antibacterial agents had come up with complete antibacterial activity as no colony could be formed in the PLCL/Z/E treated groups.

The viability of bacteria was further confirmed by live/dead staining. According the results, both strains could show proliferation on culture plates (CP) and on the surface of PLCL membrane. The viability of bacteria decreased on the surface of PLCL/Z and PLCL/E as we can observe mostly the dead bacteria stained as red (Figs. S3 and S4). The viability of bacteria further decreased on the surface of PLCL/Z/E membrane confirming the effectiveness of this membrane against both the strains (Figs. S3 and S4).

SEM images were taken to observe the growth and morphology of bacterial colonies on the surface of various NF membranes and results are shown in Fig. 5B. Notably, both the strains, *E. coli* and *S. aureus*, exhibited normal colony formation (indicated by purple arrowhead) with typical rod-like (*E. coli*) and spherical shape (*S. aureus*) which indicate that PLCL membrane had no adverse effect on bacterial growth. In contrast, the structural integrity of bacterial colonies was greatly affected on the surface of PLCL/Z, PLCL/E, and PLCL/Z/E NF membranes. Colonies were found deformed and collapsed as indicated by the blue arrowhead. Interestingly, ZnO NP was found attached on the surface of a bacterial cell in both PLCL/Z and PLCL/Z/E as indicated by the red arrowhead.

### 7.3. Antioxidant activity

The antioxidant activity of PLCL, PLCL/Z, PLCL/E, and PLCL/Z/E

was determined through DPPH radical scavenging assay. Ascorbic acid was taken as a standard antioxidant agent. According to the results exhibited in Fig. 5B, the antioxidant activities remained 82, 2, 18, 72, and 65 (%) for ascorbic acid, PLCL, PLCL/Z, PLCL/E, and PLCL/Z/E respectively. A representative image of various experimental samples is also provided to observe color changes due to radical scavenging activity. When radical scavenging takes place, the typical purple color disappeared indicating the antioxidant activity. We can see both PLCL/E and PLCL/Z/E had substantial antioxidant activity. These results indicated that only NF membranes containing OEO exhibited strong antioxidant activity arguing the fact that antioxidant activity was only associated with OEO.

### 7.4. In vitro cell culture

Various cell culture attributes such as proliferation, cell viability, adhesion, and cellular morphology were assessed through CCK-8, live/dead staining, F-actin/DAPI staining, and SEM analysis. CCK-8 assay was employed on days 1, 4, and 7 to assess the viability of the cells. The absorption at 450 nm is proportional to the number of viable cells. According to Fig. 6A, PLCL/E showed the maximum cell growth ad PLCL/Z was the lowest among the fabricated NF membrane. The addition of ZnO reduced the number of NIH-3T3 but the growth of the cells continued for 7 days on all samples indicated that the membranes were slight to non-cytotoxic. The trend of cell growth can be co-related to the hydrophilicity of the membrane and the presence of ZnO. Moreover, results showed that the used concentrations of ZnO and OEO were not cytotoxic. The viability of cells was also assessed by live/dead staining. Green stained indicated living cells, whereas, red-stained indicated dead cells. We could see very few red-stained cells indicating the very low toxicity of all fabricated membranes (Fig. S7).

The adhered cell morphology was assessed by F-actin/DAPI staining. The result indicated that the shape of the cells was normal and cells were well adhered to and increasing their number. The cytoskeletal network was well established having blue-stained round nuclei (Fig. 6B). The adhesion of cells was also assessed by SEM and results indicated that all the nanofibrous membrane support cell adhesion on their surfaces (Fig. 6C). The biocompatibility of the NF membranes makes them a potential wound dressing candidate.

## 8. In vivo experiment

### 8.1. Wound healing assessment

Skin defects were created in diabetic rats to assess the wound healing potential of fabricated NF membranes. An untreated group (only covered with gauze) was taken as a control for comparison as shown in Fig. 7A. Fig. 7B is the representative graph displaying the healing progress at days 05, 10, and 15. On day 05, all the groups, treated with the NF membrane, showed significantly different ($p < 0.05$) healing compared to the untreated. On day 10, bioactive NF membranes PLCL/Z, PLCL/E, and PLCL/Z/E showed a significant increase in wound closure. This impact pattern of various NF membrane continued for 15 days. All the bioactive NF membranes could close the wound by more than 80% each including PLCL/Z/E which showed about 89.7% wound closure on day 15. Fig. 7C is the representative image showing the

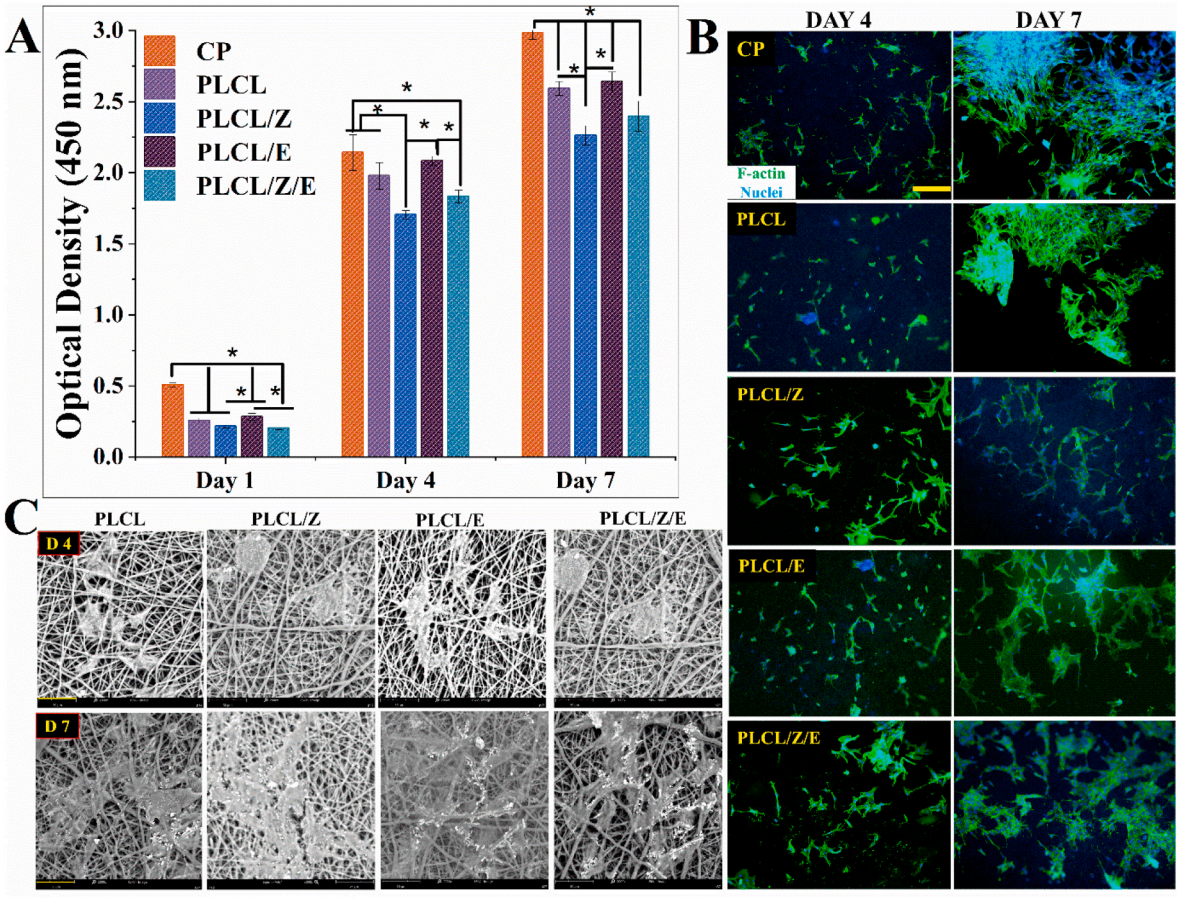


**Fig. 6.** Representative image showing the results of in vitro cell culture (A) graph of CCK-8 results showing the absorbance proportional to the viability of NIH-3T3 cells, (B) fluorescent images showing F-actin/DAPI staining at day 4 and 7 (scale bar = 200 μm), (C) SEM images, showing the growth of NIH-3T3 cells on NF membrane, taken at day 4 and 7 (scale bar = 30 μm). Statistical analysis was performed by one-way ANOVA followed by Tukey's multiple comparison test, n = 3, *$p < 0.05$.

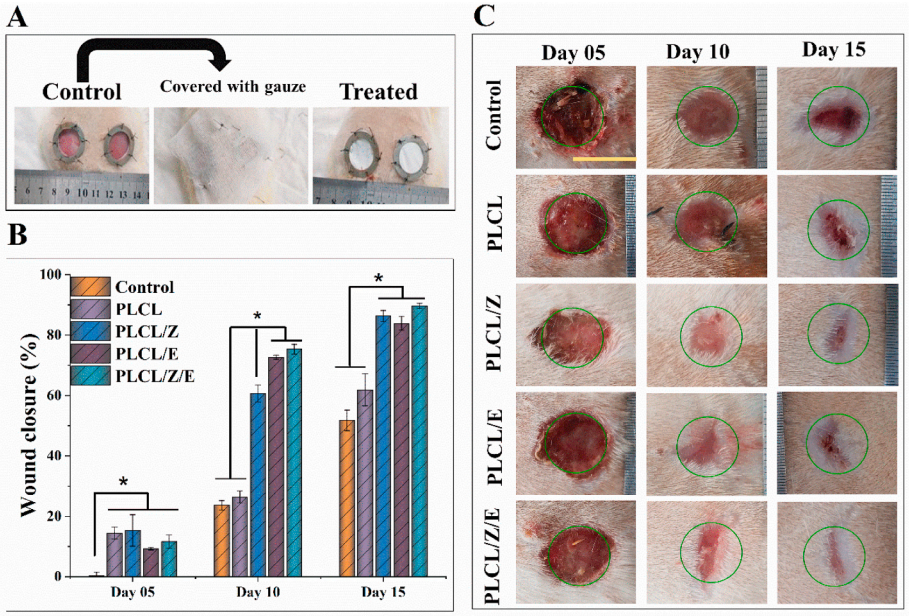


**Fig. 7.** Image showing the application of various nanofibrous membrane on diabetic wound model (A) Image showing the wound sutured with stainless steel and placement of the NF membrane on a wound, (B) representative graph of wound closure (%) measured at day 05, 10, and 15, (C) image showing the progress of wound closure in untreated (control) and treated with various NF membranes taken at 5,10 and 15 D time points (scale bar = 18 mm). Statistical analysis was performed by one-way ANOVA (*$p < 0.05$).

progress of healing noted at various time times. we can also observe the clarity in the wound area, free from debris, exhibiting the capability of the electrospun NF membrane in absorbing the wound exudates.

### 8.2. Histological staining

Masson's trichrome stain of various tissues taken from the wound bed along with surrounding healthy skin tissue is shown in Fig. 8. Both the untreated group and group treated with PLCL NF membrane could not overcome inflammation, marked with the blue arrow, throughout the monitored period. In contrast, all bioactive NF membranes such as PLCL/Z, PLCL/E, and PLCL/Z/E showed no sign of inflammation observed on day 10 and 15 (Fig. 8, Fig. S6). A slight inflammation, however, was observed on the 5th day which was part of a normal healing process (Fig. S6). These observations indicated that PLCL/Z, PLCL/E, and PLCL/Z/E reduced inflammation in wounds. Moreover, these images demonstrated the non-existence of epithelialization in the untreated group. Whereas, a partial epithelial layer was observed in the PLCL treated group. PLCL/Z, PLCL/E, and PLCL/Z/E treated wound had complete epithelialization with intact stratum corneum and stratum basale on day 15 (dark and light green arrows, Masson,s staining). Moreover, collagen deposition was very thin and unorganized in an untreated group. Whereas, the NF membrane treated group had more collagen deposition especially the group treated with PLCL/Z and PLCL/Z/E. Among all, PLCL/Z/E treated group had more and highly organized collagen fibers (black arrow). A similar trend was also observed for neovascularization and PLCL/Z/E treated group had more angiogenesis and a better network of capillaries (pink arrow). Fig. S6 indicates that tissue organization was started with 10 days, in a group treated with PLCL/Z and PLCL/Z/E (yellow circle). The organization further improved up to 15 days and the presence of the sebaceous gland could be traced (Fig. 8 yellow circle). Moreover, to draw a better comparison between newly formed tissues and neighboring skin, both were indicated by yellow and red boxes respectively (Fig. 8). All these indicators confirmed that the bioactive NF membranes demonstrated the potential of new tissue formation in DW.

H&E staining was also performed to observe the granulation tissue formation. The H&E staining depicted the granulation and cellular migration from margin to center. Fig. S7 indicated neutrophilic accumulation, stained as dark blue cell clusters, in all the membranes at day 5 (yellow arrow). But that inflammatory activity reduced drastically in PLCL/Z/E treated group on day 10 and the scar was replaced by newly formed epithelium (green arrow). The cluster of neutrophilic cells can also be observed in untreated and PLCL treated groups indicating the ongoing inflammatory activity (black circle). Whereas, bioactive treated groups had overcome the inflammation (Fig. 8, H&E staining). The untreated group had still an incomplete epidermis (orange line) after 15 days confirming the slow healing in DW. Whereas, almost complete granulation is observable in groups treated with NF membranes. H&E stains also confirmed the organization of collagen fibers in newly formed tissues treated with various NF membranes. A much organized, fiber-shaped, and loosely packed, collagen (Fig. 8 light green circle, H&E staining) was observed in PLCL/Z and PLCL/Z/E treated wound exhibiting the potential of these membranes in the quality of wound healing.

### 8.3. Immunohistochemical staining

Immunohistochemical staining was employed to assess the VEGF expression in wounds on days 10 and 15. Fig. 9 is the representative image of histochemical stains of tissues taken from the wound bed of untreated and treated with various NF membranes. These results demonstrated a weak positive VEGF staining in the untreated group. Whereas, comparatively, strong positive VEGF staining can be observed in PLCL treated group on day 15 (red arrowhead). We can also observe the epithelial layers counterstained with hematoxylin especially in untreated and PLCL treated groups indicating the non-existence of mature epithelia at these time points. PLCL/Z treated group also had a strong expression of VEGF resulting in a higher number of blood vessels at both time points (red arrowhead). This indicated that ZnO NP could induce angiogenesis in DW. Although granulation and epithelialization were complete in the group treated with PLCL/E yet the expression of VEGF was very weak especially on the 10th day. The PLCL/Z/E treated group showed the best VEGF expression at both time points. On the 15th day, the vessels looked mature with a visible lumen (red arrowhead). The strong expression of VEGF, in the group treated with PLCL/Z/E compared to PLCL/Z and PLCL/E, proved the hypothesis that co-delivery of two bioactive agents could act synergistically to promote angiogenesis.

### 8.4. Fluorescence quantitative PCR

Fluorescent quantitative PCR was employed to get an idea of the

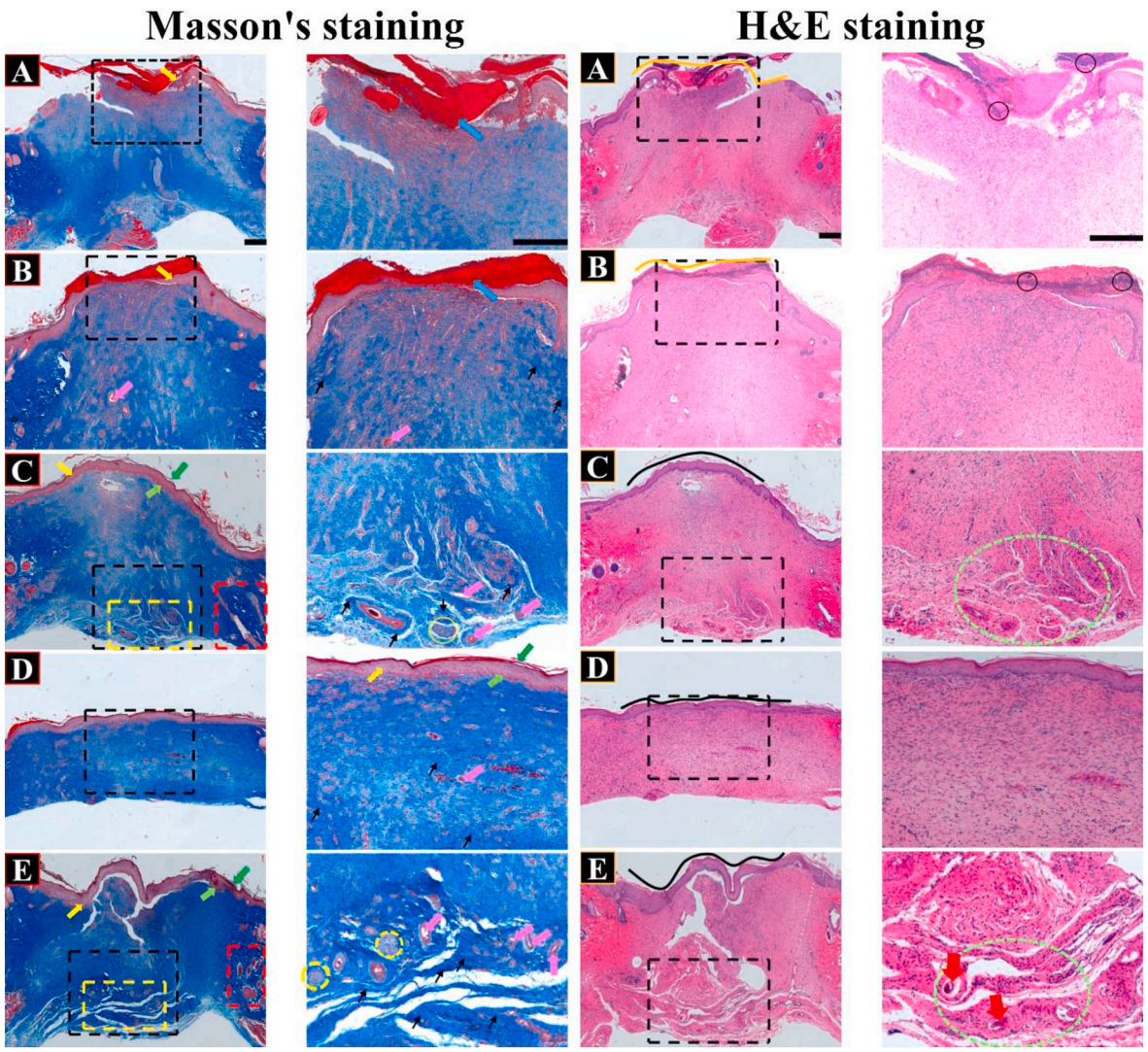


**Fig. 8.** Fluorescent image of tissues stained with Masson's trichrome and H&E stain at day 15 along with a magnified portion selected in the dotted square. (scale bar = 200 μm). (A, B, C, D, and E representing untreated, PLCL, PLCL/Z, PLCL/E, and PLCL/Z/E treated respectively). In Masson's staining, the epithelial layer, stratum corneum, stratum basale, inflammation, mature collagen fibers, blood vessels, sebaceous glands, tissue maturation in the wound area, original tissues indicated by the yellow arrow, dark green arrow, light green arrow, blue arrow, black arrow, pink arrow, and yellow dotted circle, yellow dotted box, and red dotted box respectively. In H&E staining, incomplete epithelialization, complete epithelialization, neutrophilic, tissue organization, and blood vessels are indicated with the orange line, black line, black circle, green dotted circle, and red arrow respectively. (For interpretation of the references to color in this figure legend, the reader is referred to the Web version of this article.)

underlying mechanism of wound healing, treated with different NF membranes. IL-6 and MMP-9 are two inflammation related genes and their expression was quantified in newly formed tissues. Fluorescent quantitative PCR demonstrated a highly similar pattern of mRNA expressions for both IL-6 and MMP-9 genes (Fig. 10A and B). The untreated wound exhibited an elevated level of IL-6 and MMP-9 which indicated inflammation in the wound area. PLCL NF membrane treated group also had an elevated quantity of both mRNAs. Whereas, bioactive NF membrane wounds had significantly dropped the IL-6 and MMP-9 related RNAs which indicated that the rapid wound healing was associated with the downregulation of pro-inflammatory cytokines leading to the termination of the inflammatory phase.

## 9. Discussion

Wound healing is a comprehensive mechanism regulated by various growth factors and cytokines produced by a variety of cell types such as endothelial, fibroblasts, phagocytes, and platelets at various stages of healing [41]. DW, however, exhibits impaired response to these growth factors and cytokines due to various microvascular complications and infiltrations of inflammatory cells leading to an unending inflammatory cycle. Lack of angiogenesis due to hyperglycemia results in ischemia which is a major cause of oxygen and nutrient deprivation in growing cells and tissues. Moreover, glycation of hemoglobin leads to tissue hypoxia, a signal for ROS generation. The excessive release of ROS results in the breakdown of ECM and granulation tissues [42]. Besides, infection is also the most prevalent factor in DW. For an active wound dressing aimed to manage DW complications, it must be capable to promote angiogenesis, neutralize ROS, combat microbial invasion as a well strong anti-inflammatory effect. Along with this, healing related micronutrient supplements can accelerate the healing process. Considering the DW complications in the account, we developed a multifunctional dual bioactive agent loaded composite electrospun NF membrane capable to promote vascularization, downregulating inflammatory-related genes, scavenging the free radicals, and cleaning the wound from pathogens as well as absorbing wound exudates.

The basic aim of the study was to make possible the co-delivery of ZnO NP and OEO to DW. In this study, we combined two conventional

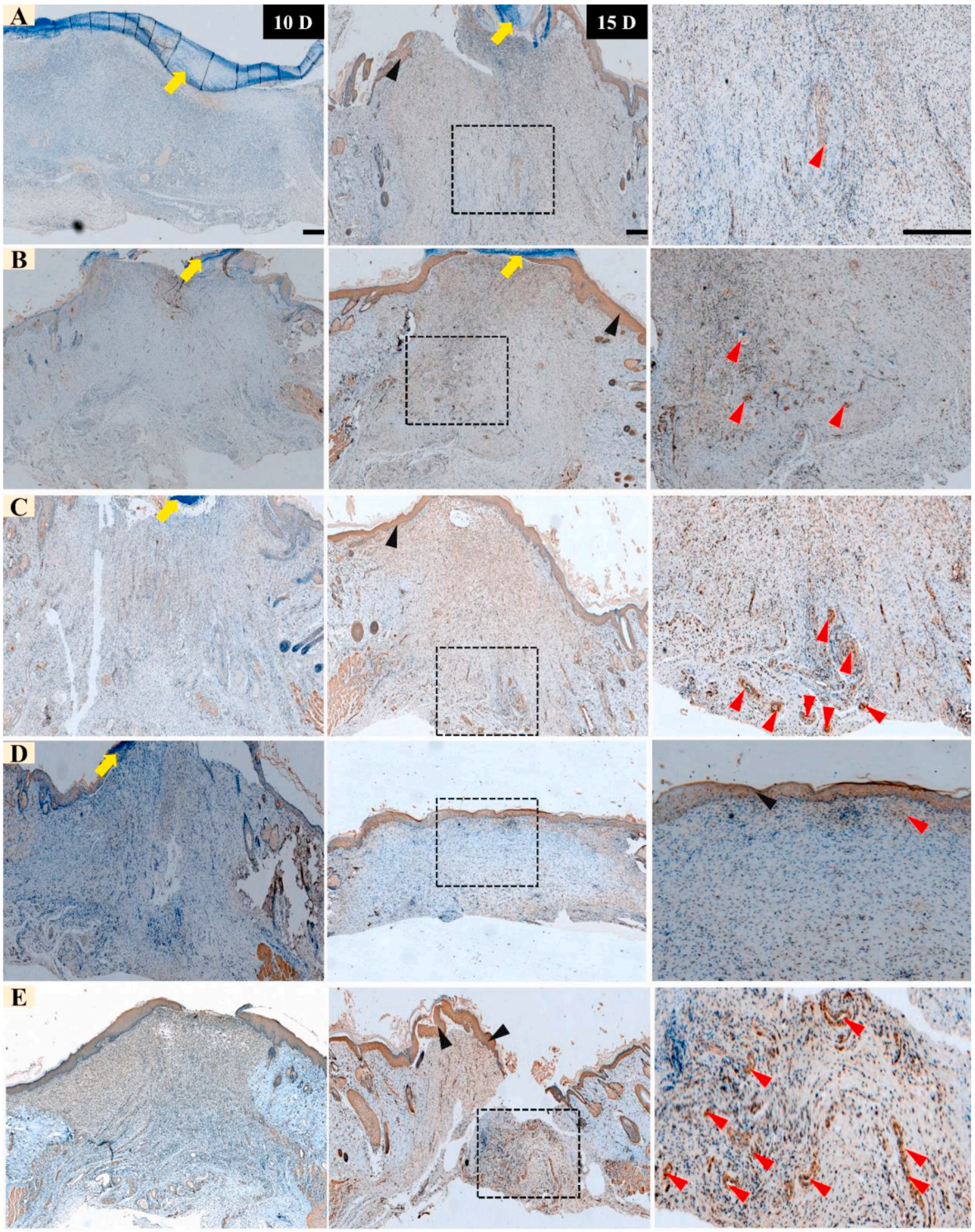


**Fig. 9.** Immunohistochemical staining of VEGF at days 10 and 15 and magnified portion, shown in the dotted square. (A, B, C, D, and E representing untreated, PLCL, PLCL/Z, PLCL/E, and PLCL/Z/E treated respectively) (scale bar = 200 μm). Hematoxylin counterstained epidermis, VEGF positive stain of the epidermis, thick VEGF-stained tissues in the wound area are indicated by the yellow arrow, black arrowhead, and red arrowhead respectively.

techniques for loading bioactive agents into electrospun nanofibers. Emulsion electrospinning and core-shell electrospinning are two widely used methods for loading bioactive compounds which are either meant for the controlled release of bioactive agents or protect them from the harmful effect of organic solvents. Both these conventional techniques have been employed for loading essential oils in nanofibers [43,44]. We adopted a new strategy for loading volatile compounds and demonstrated the controlled release. Firstly, we made the oil in water emulsion stabilized by surfactant and later on, loaded into the core of the nanofiber through the core-shell electrospinning technique as shown in Fig. 1A. This provided an additional layer around the OEO. Moreover, the core-shell structure enabled us to load another bioactive substance separately in the shell of the fiber. We selected PLCL, a highly promising synthetic polymer with the remarkable mechanical property. However,

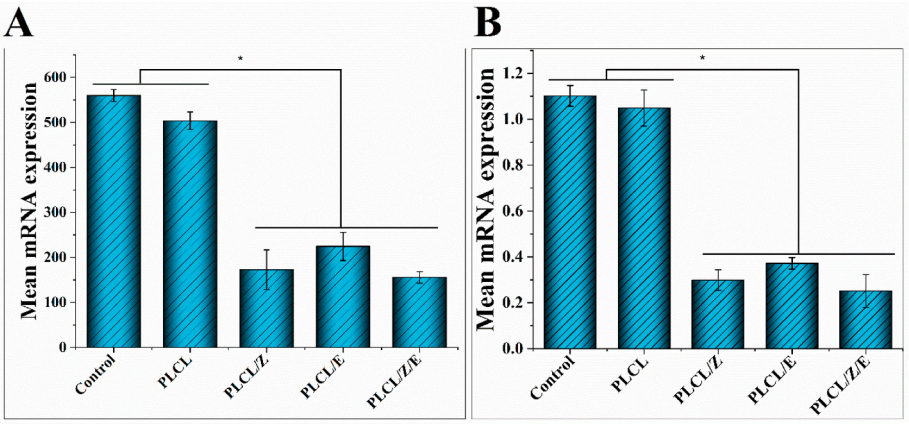


**Fig. 10.** Representative image showing fluorescence quantitative PCR (A) The graph representing the mRNA expression for IL-6 gene, (B) mRNA expression of MMP-9 gene in the untreated wound, and treated with NF membranes at day 10. Statistical analysis was performed by one-way ANOVA followed by Tukey's multiple comparison test, n = 3, $*p < 0.05$.

its weak wettability may be disadvantageous as a dressing material. To tackle the wettability, we made the emulsion in hyaluronic acid solution to be used in the core. Resultantly, hydrophilicity was achieved. The detailed schematic illustration of the fabrication mechanism and types of NF membrane is shown in Fig. 1.

External and internal morphological analysis showed that the NF membrane, loaded with dual bioactive agents, could be fabricated through electrospinning. The surface roughness and large fiber diameter in PLCL/Z and PLCL/Z/E are due to loading ZnO NP which formed few agglomerates on the surface due to high surface energy. Whereas, large fiber diameter can be explained in terms of solution viscosity which increases due to the presence of nanofiller agglomerates [45]. The average diameter of the PLCL NF membrane is in agreement with the previously reported work [46]. However, a core-shell structure having oil emulsion in the core had shown the least diameter size significantly different ($p < 0.05$) from PLCL and PLCL/Z NF (Fig. 2). This difference can be mainly attributed to the relatively low flow rate of shell solution of about 1 mL/h compared to 1.2 mL/h in the case of PLCL and PLCL/Z. The ZnO NP was found evenly distributed in the fiber both within the matrix and on the surface confirmed through EDX and TEM. The average ZnO NP size, we used in our study, was about 40 nm. This study indicated that this size of NP can be encapsulated within the polymeric matrix.

Wettability is a desirable feature for a wound dressing. A dressing with hydrophilic nature can easily absorb the wound exudates thus clean the wound from any debris. PLCL is a hydrophobic polymer [30]. Our core-shell NF membranes showed better wettability due to hyaluronic acid in the core. However, PLCL/Z/E exhibited comparatively low hydrophilicity mainly due to the addition of ZnO (Fig. 3B). The water contact angle for PLCL/Z/E is ideal for wound dressing because the contact angle around 70° may help absorb cell adhering proteins leading to better cell attachment [47].

Sustained release of a bioactive substance is another desirable feature for a drug-loaded scaffold. Our release profile for both ZnO and OEO, measured for 3 days, demonstrated the biphasic release of these substances (Fig. 3). The initial burst release followed by sustained release. The mechanism of ZnO release mainly included desorption, diffusion as well as break down of fiber. Interestingly, there was a marginal difference noted in the amount of $Zn^{+2}$ release from PLCL/Z and PLCL/Z/E, although both membranes contained the same amount of ZnO NP. The more release of $Zn^{+2}$ from the PLCL/Z/E membrane can be attributed to its hydrophilic nature due to the presence of hyaluronic acid (HA) in the core (Fig. 3B). Absorbed water contents lead to the swelling of nanofiber opening the channel for $Zn^{+2}$ release. Our hypothesis to encapsulate OEO within the core of the fiber having two-layered protection enabled us to get a sustained release of the volatile compound. This is a modified loading strategy and can be used to encapsulate the volatile compounds in future researches too. The initial burst release is beneficial with an aspect to combat the infiltrating pathogens in an open wound.

A suitable mechanical strength is also a pre-requisite for the practicability of a wound dressing. A wound dressing aimed for skin regeneration should have at least 1–32 MPa of mechanical strength and 17–207% elongation at break [48]. In our case, the addition of ZnO affected the mechanical strength mainly due to the weak interaction of ZnO and PLCL (Fig. 4). This weak interaction led to the weakening of the fiber strength of PLCL resulted in slightly reduced mechanical strength. Moreover, the tensile strength and young's modulus was also correlated with the fiber diameter. PLCL/E NF membrane had tensile strength insignificantly different ($p < 0.05$) form PLCL. However, it's young's modulus was highest among all. The higher tensile strength and young's modulus can be attributed to a fine fiber structure. A finer diameter possesses a densely packed fibrillar structure resulting in high resistance to an axial tensile force. Whereas, this orientation loses with increasing fiber diameter resulting in low tensile strength [49]. Despite these facts, all the NF membranes showed enough tensile strength and strain required for skin tissue regeneration.

Slow closure of DW makes it prone to develop the infection [50]. A wound dressing meant to heal DW should have antimicrobial potential. The use of conventional antibiotics may pose a risk of bacterial resistance. We employed an idea of combining two antibacterial agents, oregano essential oil and ZnO NP, both have established antibacterial activity, to clear the wound from any infection. In this study, we selected two model bacteria, *E. coli* and *S. aureus*, representing gram-negative and gram-positive respectively, to study the in vitro antibacterial potential of various nanofibrous membranes. However, studies indicate that *pseudomonas aeruginosa* is another common bacterium, along with *staphylococcus aureus* and *E. coli* in diabetic foot ulcers [51–53]. Although, we could not test our fabricated nanofibrous membrane against *P. aeruginosa.* literature reports the effectiveness of both ZnO NP and OEO against this bacterium [53–56]. Many studies reported the effectiveness of OEO against multidrug resistance (MR) bacterial strain [57]. Earlier OEO was combined with silver NP and synergy between two agents was achieved against MRSA [58]. Similarly, carvacrol was combined with ZnO NP and this combination was found highly effective against *Campylobacter jejuni*. Moreover, it was also observed that a single treatment with one antibacterial agent, in low concentration, could show bacteriostatic effect [59]. The idea of combining essential oil with ZnO NP enabled us to use antibacterial agents in low concentrations to ensure biocompatibility.

Maximum antibacterial activity (%) was observed in groups treated with PLCL/Z/E which was further supported by turbidity analysis as

shown in Fig. 5A and Fig. S1 respectively. The decrease of viability of bacteria on the surface of bioactive NF membrane (PLCL, PLCL/Z and PLCL/Z/E) was further confirmed by live/dead staining (Figs. S3 and S4). Almost complete loss of viability of both strains on the surface of PLCL/Z/E indicates the antibacterial potential of the membrane. SEM observation of bacterial colonies further verified that intact colonies could only be formed on the surface of the PLCL NF membrane. Whereas, a great inhibition of bacterial colonies and deformation of cells were observed in groups cultured on the surface on bioactive membranes (Fig. 5B). The deformed colonies provide preliminary evidence that the impact of bioactive NF membranes was microbiocidal which remained more prominent in the case of PLCL/Z/E indicating the synergy between these two agents. The microbiocidal impact of this antimicrobial combination can be explained in terms of the lipophilic attraction of OEO to the cell membrane of bacteria. The inclusion within the bacterial membrane causes membrane expansion and permeability. This itself causes the inhibition of respiration and disturbance in the ion-exchange channel along the membrane [60]. Moreover, this permeable membrane facilitated ZnO NP to enter into the cytoplasm destroying it by generating ROS, a major mechanism of action of ZnO NP [61]. This study also demonstrated that a combination of two antibacterial agents, with synergistic action, can be another option to avoid the toxic effects of antibacterial agents and also minimizes the chance of developing bacterial resistance against high doses.

One of the great challenges, a DW face is the uncontrolled production of ROS [62]. The excessive ROS generation correlates with impaired wound healing. The ROS mediated transcription results in the production of proinflammatory cytokines and the induction of MMPs. Keeping the ROS level at low concentration is essential to resume the healing process. Researchers have successfully used various antioxidant agents to mitigate the problem of ROS thus promoting the healing in DW [12,63]. Our multipronged strategy included the scavenging of these ROS through an antioxidant agent to terminate the inflammatory phase. According to antioxidant activity results, the NF membrane containing oil emulsion showed ROS scavenging which means that OEO within oil emulsion has antioxidant activity (Fig. 5B). OEO contains two major components carvacrol and thymol which are capable to donate a hydrogen atom to free radicals converting to nonradical products with the help of many phenolic compounds [64].

Since the wound dressing has to come in close contact with body tissues, its biocompatibility is highly required. The adhesion and proliferation of NIH-3T3 fibroblast cells in all of the NF membranes showed the biocompatibility of the NF membranes. The trend of cell proliferation correlates with the presence of ZnO NP and hydrophilicity of NF membranes. In a previous study conducted by Stephan Hackeberg et al., the cytotoxicity and genotoxicity of ZnO NP were reported. The cytotoxic quantity was identified as 50 μg/mL for nasal mucosa cell line [65]. Another recent study reported ZnO NP associated cytotoxicity against mouse ovarian germ cells and a significant reduction in cell viability when grown in culture media with 30 μg/mL compared to 10 and 20 μg/mL [66]. In conclusion, the cytotoxicity of ZnO NP largely varies with varying particle size, surface properties, and tested cell lines [26,65]. However, one of the advantages, nanofibers possess, is to deliver the bioactive agent sustainedly to avoid the possible toxic effect due to direct exposure to overdose. Many previous studies reported the biocompatibility of ZnO loaded electrospun nanofibers in low concentrations [26,67]. Our result, however, showed a slight reduction in viable NIH-3T3 cells when cultured on PLCL/Z/E membrane but the viability of NIH-3T3 cells was significantly higher ($p < 0.05$) than PLCL/Z. The difference can be attributed to improved hydrophilicity of the PLCL/Z/E membrane. PLCL and PLCL/E showed maximum proliferation due to smooth surface and good hydrophilicity in the case of PLCL/E. In conclusion, all the NF membranes supported cell adhesion and proliferation with a normal cytoskeletal network which was further confirmed by F-actin/DAPI and SEM images (Fig. 6).

Electrospun NF membranes possess some special structural features such as porosity, ECM-like network, the capability to exchange gases, moisture-retaining, and absorption of exudates which makes them ideal wound dressing materials. If the NF membranes are loaded with active agents, the impact on wound healing can be magnified. We established a type-1 diabetic wound model to better understand the healing potential of various NF membranes in complicated wounds. Histological staining confirmed the closure of the wound was associated with epithelialization and no apparent sign of scar left in the wound treated with the bioactive membrane (Fig. 8). Masson's trichrome and H&E staining exhibited that both ZnO NP and OEO can promote angiogenesis, epithelialization, and granulation. Prolonged inflammation, due to earlier mentioned factors, is the hallmark of DW. The wound healing induced by bioactive NF membranes is mainly due to anti-inflammatory and antioxidant effects. We see no signs of inflammation in wounds treated with PLCL/Z, PLCL/E, and PLCL/Z/E at 10th and 15th day time points (Fig. S6, Fig. 8). The healing quality, in terms of complete epithelialization, neo-vascularization, granulation, and collagen deposition is more evident in the group treated with PLCL/Z/E demonstrating that co-delivery of ZnO NP and OEO can synergistically promote these wound-healing attributes.

In DW, reduced expression of VEGF and its proteolytic degradation is another major cause of impaired wound healing [68,69]. Since VEGF expression is directly related to angiogenesis, a poor network of blood capillaries prevents the proper supply of nutrients and oxygen to granulation tissues. Increasing the VEGF expression can help promote its response and resultantly neo-vascularization. The vascular network is highly significant in stimulating, mobilization, and recruitment of endothelial cells which ultimately assemble to form blood vessels. Moreover, blood profusion and metabolism are also promoted by increased capillary density as a result of VEGF expression. From the immunohistochemical staining, we can analyze that two treated groups, PLCL/Z and PLCL/Z/E showed maximum vascularization followed by PLCL/E and PLCL. The visible thick vessels in the group treated with PLCL/Z/E showed that this NF membrane was capable to promote angiogenesis (Fig. 9). The ability of Zn containing biomaterials to induce angiogenesis via VEGF expression is in confirmation with previously reported work [26,70]. From the VEGF immunohistochemical staining, we can conclude that the bioactive NF membrane could promote the granulation, collagen deposition, and epithelialization via vascular network formation.

Prolonged inflammation is the ultimate cause of delayed DW healing [71]. One of the key bioactivities features desired for an active wound dressing is the anti-inflammatory effect. The underlying mechanistic insight of the anti-inflammatory effect of the bioactive NF membrane was confirmed through fluorescent quantitative PCR. IL-6 and MMP-9 are two important genes in which expression is related to the release of proinflammatory cytokines [72,73]. These two cytokines are present at elevated levels in DW, a major cause of delayed wound healing [73]. Hyperglycaemia has been shown to elevate the IL-6 level thus a strong correlation is always found between DFU and elevated level of IL-6 [74]. Therefore, reducing the IL-6 level employing antibody-mediated or natural treatment can be a detrimental factor for DW healing. Quantitative PCR demonstrated that the IL-6 level was drastically down-regulated by bioactive NF membranes especially PLCL/Z and PLCL/Z/E (Fig. 10A). MMP-9 related enzymes are major factors contributing to the destruction of ECM [74]. Previous studies revealed that the level of MMPs in DW is 60% more than in an acute wound [75]. Like IL-6, a strong correlation between impaired wound healing and the elevated level of MMP-9 is also evident. The destruction of the ECM network retards the granulation process. The proposed bioactive NF membrane also significantly down-regulated the MMP-9 related gene thus decreasing its level (Fig. 10B).

Based on the outcomes of the study, we can project the possible mechanism of action of bioactive NF membrane, especially PLCL/Z/E, when applied on a wound as illustrated in Fig. 11. The initial role played by the NF membrane was to protect against any possible microbial

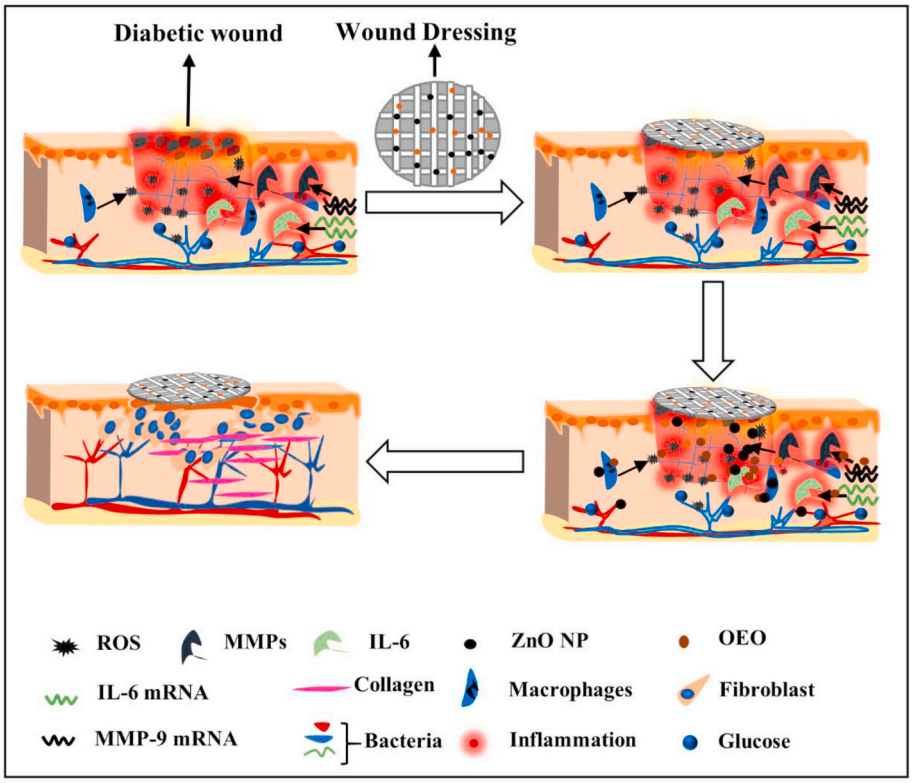


**Fig. 11.** Schematic illustration of the mechanism of action of the proposed wound dressing on the diabetic skin wound model.

invasion. Their permeability for the exchange of gases and the absorption of wound exudates also positively affected the initial healing process. Moreover, the microenvironment allowed cellular migration and proliferation thus helped in granulation tissue formation. The major role played in granulation was the promotion of angiogenesis. Besides, radical scavenging also helped in balancing the level of ROS which improved the healing process. More importantly, the inflammatory cycle was terminated by bioactive NF membranes by downregulating the pro-inflammatory cytokines related gene expression.

Although, we substantially characterized the NF membranes and evaluated in vitro and in vivo performance, more thorough investigation is still required to investigate the possible cytotoxic effect of membranes on other relevant cell lines. Moreover, a diabetic wound model, with established biofilm, is also required to assess the in vivo antibiofilm performance. This study somehow provides preliminary evidence of angiogenesis and anti-inflammatory activities, however, a detailed underlying mechanistic insight is still required before considering the membrane for clinical use.

## 10. Conclusion

In summary, we developed a multifunctional core-shell NF membrane loaded with two bioactive agents (ZnO NP and OEO) for the healing of DW. We used a modified loading strategy of OEO, a volatile compound, into the core of the fiber in the form of oil in water emulsion and made possible the controlled release. The two bioactive agents acted synergistically to show strong antibacterial potential. Bioactive membranes also successfully closed the wound with complete epithelialization, granulation tissue formation, neo-vascularization, and collagen deposition. We have seen a great vascularization in wounds treated with PLCL/Z/E with highly organized collagen fibers. The angiogenetic potential of the bioactive NF membranes was confirmed through VEGF expression. Moreover, the bioactive NF membranes had shown an anti-inflammatory effect by down-regulating inflammatory-related gene expression. Thus, we can conclude That PLCL/Z/E, a dual bioactive agent loaded electrospun NF membrane, is capable to promote DW due to its anti-bacterial, antioxidant and anti-inflammatory potentials.

## Declaration of competing interest

The authors declare that they have no known competing financial interests or personal relationships that could have appeared to influence the work reported in this paper.

## CRediT authorship contribution statement

**Atta ur Rehman Khan:** Investigation, Formal analysis, Writing - original draft. **Kai Huang:** Investigation. **Mina Shahriari Khalaji:** Investigation. **Fan Yu:** Conceptualization. **Xianrui Xie:** Conceptualization. **Tonghe Zhu:** Formal analysis. **Yosry Morsi:** Conceptualization, Formal analysis. **Zhao Jinzhong:** Resources, Supervision. **Xiumei Mo:** Supervision, Project administration, Funding acquisition, Writing - review & editing.

## Acknowledgment

This research was supported by the Fundamental Research Funds for the Central Universities (2232019A3-07), National Key Research Program of China (2016YFC1100202), National Natural Science Foundation of China (No.31771023), Science and Technology Commission of Shanghai Municipality (No.19441902600, 20S31900900).

## Appendix A. Supplementary data

Supplementary data to this article can be found online at https://doi.org/10.1016/j.bioactmat.2021.01.040.

## References


[1] I.D. Federation, Diabetes Facts & Figures, 2019, 2019, http://www.idf.org/aboutdiabetes/what-is-diabetes/facts-figures.htmL. (Accessed 10 August 2020).

[2] K. Singh, C.K. Sen, Chapter 9 - epigenetics of diabetic wound healing, in: D. Bagchi, A. Das, S. Roy (Eds.), Wound Healing, Tissue Repair, and Regeneration in Diabetes, Academic Press, 2020, pp. 167–180.

[3] U. Freudenberg, A. Zieris, K. Chwalek, M.V. Tsurkan, M.F. Maitz, P. Atallah, K. R. Levental, S.A. Eming, C. Werner, Heparin desulfation modulates VEGF release and angiogenesis in diabetic wounds, J. Contr. Release 220 (Pt A) (2015) 79–88.

[4] S.M. Choi, K.-M. Lee, H.J. Kim, I.K. Park, H.J. Kang, H.-C. Shin, D. Baek, Y. Choi, K. H. Park, J.W. Lee, Effects of structurally stabilized EGF and bFGF on wound healing in type I and type II diabetic mice, Acta Biomater. 66 (2018) 325–334.

[5] P. Losi, E. Briganti, C. Errico, A. Lisella, E. Sanguinetti, F. Chiellini, G. Soldani, Fibrin-based scaffold incorporating VEGF- and bFGF-loaded nanoparticles stimulates wound healing in diabetic mice, Acta Biomater. 9 (8) (2013) 7814–7821.

[6] V. Kant, D. Kumar, R. Prasad, A. Gopal, N.N. Pathak, P. Kumar, S.K. Tandan, Combined effect of substance P and curcumin on cutaneous wound healing in diabetic rats, J. Surg. Res. 212 (2017) 130–145.

[7] S. Hamed, Y. Ullmann, D. Egozi, E. Daod, E. Hellou, M. Ashkar, A. Gilhar, L. Teot, Fibronectin potentiates topical erythropoietin-induced wound repair in diabetic mice, J. Invest. Dermatol. 131 (6) (2011) 1365–1374.

[8] C.H. Lee, K.C. Hung, M.J. Hsieh, S.H. Chang, J.H. Juang, I.C. Hsieh, M.S. Wen, S. J. Liu, Core-shell insulin-loaded nanofibrous scaffolds for repairing diabetic wounds, Nanomedicine 24 (2020) 102123.

[9] S. Cui, X. Sun, K. Li, D. Gou, Y. Zhou, J. Hu, Y. Liu, Polylactide nanofibers delivering doxycycline for chronic wound treatment, Mater. Sci. Eng. C 104 (2019), 109745.

[10] S. Tort, F.T. Demiröz, Ş. Coşkun Cevher, S. Sarıbaş, C. Özoğul, F. Acartürk, The effect of a new wound dressing on wound healing: biochemical and histopathological evaluation, Burns 46 (1) (2020) 143–155.

[11] R. Ahmed, M. Tariq, I. Ali, R. Asghar, P. Noorunnisa Khanam, R. Augustine, A. Hasan, Novel electrospun chitosan/polyvinyl alcohol/zinc oxide nanofibrous mats with antibacterial and antioxidant properties for diabetic wound healing, Int. J. Biol. Macromol. 120 (2018) 385–393.

[12] A. Burns, W.T. Self, 11 - antioxidant inorganic nanoparticles and their potential applications in biomedicine, in: G. Ciofani (Ed.), Smart Nanoparticles for Biomedicine, Elsevier2018, pp. 159-169.

[13] R. Augustine, A. Hasan, N.K. Patan, Y.B. Dalvi, R. Varghese, A. Antony, R.N. Unni, N. Sandhyarani, A.-E.A. Moustafa, Cerium oxide nanoparticle incorporated electrospun poly(3-hydroxybutyrate-co-3-hydroxyvalerate) membranes for diabetic wound healing applications, ACS Biomater. Sci. Eng. 6 (1) (2020) 58–70.

[14] F. Liu, X. Li, L. Wang, X. Yan, D. Ma, Z. Liu, X. Liu, Sesamol incorporated cellulose acetate-zein composite nanofiber membrane: an efficient strategy to accelerate diabetic wound healing, Int. J. Biol. Macromol. 149 (2020) 627–638.

[15] A.D. Pinzón-García, P. Cassini-Vieira, C.C. Ribeiro, C.E. de Matos Jensen, L. S. Barcelos, M.E. Cortes, R.D. Sinisterra, Efficient cutaneous wound healing using bixin-loaded PCL nanofibers in diabetic mice, J. Biomed. Mater. Res. B Appl. Biomater. 105 (7) (2017) 1938–1949.

[16] Y.C. Shin, D.-M. Shin, E.J. Lee, J.H. Lee, J.E. Kim, S.H. Song, D.-Y. Hwang, J.J. Lee, B. Kim, D. Lim, S.-H. Hyon, Y.-J. Lim, D.-W. Han, Hyaluronic acid/PLGA core/shell fiber matrices loaded with EGCG beneficial to diabetic wound healing, Adv. Healthc. Mater. 5 (23) (2016) 3035–3045.

[17] H. Chen, P. Jia, H. Kang, H. Zhang, Y. Liu, P. Yang, Y. Yan, G. Zuo, L. Guo, M. Jiang, J. Qi, Y. Liu, W. Cui, H.A. Santos, L. Deng, Upregulating Hif-1α by hydrogel nanofibrous scaffolds for rapidly recruiting angiogenesis relative cells in diabetic wound, Adv. Healthc. Mater. 5 (8) (2016) 907–918.

[18] X. Ren, Y. Han, J. Wang, Y. Jiang, Z. Yi, H. Xu, Q. Ke, An aligned porous electrospun fibrous membrane with controlled drug delivery – an efficient strategy to accelerate diabetic wound healing with improved angiogenesis, Acta Biomater. 70 (2018) 140–153.

[19] W. Gao, W. Jin, Y. Li, L. Wan, C. Wang, C. Lin, X. Chen, B. Lei, C. Mao, A highly bioactive bone extracellular matrix-biomimetic nanofibrous system with rapid angiogenesis promotes diabetic wound healing, J. Mater. Chem. B 5 (35) (2017) 7285–7296.

[20] F. Zafari, S. Shirian, M. Sadeghi, S. Teimourian, M. Bakhtiyari, CD93 hematopoietic stem cells improve diabetic wound healing by VEGF activation and downregulation of DAPK-1, J. Cell. Physiol. 235 (3) (2020) 2366–2376.

[21] S. Thönes, S. Rother, T. Wippold, J. Blaszkiewicz, K. Balamurugan, S. Moeller, G. Ruiz-Gómez, M. Schnabelrauch, D. Scharnweber, A. Saalbach, J. Rademann, M. T. Pisabarro, V. Hintze, U. Anderegg, Hyaluronan/collagen hydrogels containing sulfated hyaluronan improve wound healing by sustained release of heparin-binding EGF-like growth factor, Acta Biomater. 86 (2019) 135–147.

[22] J. Zhan, H. Xu, Y. Zhong, Q. Wu, Z. Liu, Surface modification of patterned electrospun nanofibrous films via the adhesion of DOPA-bFGF and DOPA-ponericin G1 for skin wound healing, Mater. Des. 188 (2020) 108432.

[23] K.J. Woo, T.-J. Lee, J.-W. Park, T.K. Kwon, Desferrioxamine, an iron chelator, enhances HIF-1α accumulation via cyclooxygenase-2 signaling pathway, Biochem Bioph Res Co 343 (1) (2006) 8–14.

[24] Q. Zhang, J.H. Oh, C.H. Park, J.H. Baek, H.M. Ryoo, K.M. Woo, Effects of dimethyloxalylglycine-embedded poly(ε-caprolactone) fiber meshes on wound healing in diabetic rats, ACS Appl. Mater. Interfaces 9 (9) (2017) 7950–7963.

[25] P.-H. Lin, M. Sermersheim, H. Li, P.H.U. Lee, S.M. Steinberg, J. Ma, Zinc in wound healing modulation, Nutrients 10 (1) (2017) 16.

[26] R. Augustine, P. Dan, A. Sosnik, N. Kalarikkal, N. Tran, B. Vincent, S. Thomas, P. Menu, D. Rouxel, Electrospun poly(vinylidene fluoride-trifluoroethylene)/zinc oxide nanocomposite tissue engineering scaffolds with enhanced cell adhesion and blood vessel formation, Nano Res 10 (10) (2017) 3358–3376.

[27] A. Punjataewakupt, S. Napavichayanun, P. Aramwit, The downside of antimicrobial agents for wound healing, Eur. J. Clin. Microbiol. Infect. Dis. 38 (1) (2019) 39–54.

[28] M.Y. Yoon, S.S. Yoon, Disruption of the gut ecosystem by antibiotics, Yonsei Med. J. 59 (1) (2018) 4–12.

[29] A.u.R. Khan, M. Nadeem, M.A. Bhutto, F. Yu, X. Xie, H. El-Hamshary, A. El-Faham, U.A. Ibrahim, X. Mo, Physico-chemical and biological evaluation of PLCL/SF nanofibers loaded with oregano essential oil, Pharmaceutics 11 (8) (2019) 386.

[30] A.u.R. Khan, K. Huang, Z. Jinzhong, T. Zhu, Y. Morsi, A. Aldalbahi, M. El-Newehy, X. Yan, X. Mo, PLCL/Silk fibroin based antibacterial nano wound dressing encapsulating oregano essential oil: fabrication, characterization and biological evaluation, Colloids Surf. B Biointerfaces 196 (2020), 111352.

[31] H. Kuang, Y. Wang, Y. Shi, W. Yao, X. He, X. Liu, X. Mo, S. Lu, P. Zhang, Construction and performance evaluation of Hep/silk-PLCL composite nanofiber small-caliber artificial blood vessel graft, Biomaterials 259 (2020), 120288.

[32] F. Li, X. Li, R. He, J. Cheng, Z. Ni, G. Zhao, Preparation and evaluation of poly(D, L-lactic acid)/poly(L-lactide-co-ε-caprolactone) blends for tunable sirolimus release, Colloid. Surface. Physicochem. Eng. Aspect. 590 (2020), 124518.

[33] S.H. Kim, S.H. Kim, Y. Jung, TGF-β3 encapsulated PLCL scaffold by a supercritical CO2-HFIP co-solvent system for cartilage tissue engineering, J. Contr. Release 206 (2015) 101–107.

[34] B.V. Nusgens, [Hyaluronic acid and extracellular matrix: a primitive molecule?], Ann. Dermatol. Venereol. 137 (Suppl 1) (2010) S3–8.

[35] S. Lee, S. Kim, J. Park, J.Y. Lee, Universal surface modification using dopamine-hyaluronic acid conjugates for anti-biofouling, Int. J. Biol. Macromol. 151 (2020) 1314–1321.

[36] J. Voigt, V.R. Driver, Hyaluronic acid derivatives and their healing effect on burns, epithelial surgical wounds, and chronic wounds: a systematic review and meta-analysis of randomized controlled trials, Wound Repair Regen. 20 (3) (2012) 317–331.

[37] C.o.-e. garden.

[38] N. Pauzi, N.M. Zain, R.V. Kutty, H. RamLi, Antibacterial and antibiofilm properties of ZnO nanoparticles synthesis using gum Arabic as a potential new generation antibacterial agent, Mater. Today (2020).

[39] M.C. Deeds, J.M. Anderson, Armstrong, D.A. Gastineau, H.J. Hiddinga, A. Jahangir, N.L. Eberhardt, Y.C. Kudva, Single dose streptozotocin-induced diabetes: considerations for study design in islet transplantation models, Lab. Anim. 45 (3) (2011) 131–140.

[40] J. Zhang, R. Zhou, C. Xiang, Q. Jia, H. Wu, H. Yang, Huangbai liniment accelerated wound healing by activating Nrf2 signaling in diabetes, Oxid. Med. Cell Longev. 2020 (2020) 4951820.

[41] I. Pastar, O. Stojadinovic, N.C. Yin, H. Ramirez, A.G. Nusbaum, A. Sawaya, S. B. Patel, L. Khalid, R.R. Isseroff, M. Tomic-Canic, Epithelialization in wound healing: a comprehensive review, Adv. Wound Care 3 (7) (2014) 445–464.

[42] S. Jhamb, V.N. Vangaveti, U.H. Malabu, Genetic and molecular basis of diabetic foot ulcers: clinical review, J. Tissue Viability 25 (4) (2016) 229–236.

[43] C. Zhang, F. Feng, H. Zhang, Emulsion electrospinning: fundamentals, food applications and prospects, Trends Food Sci. Technol. 80 (2018) 175–186.

[44] I.M. Martins, M.F. Barreiro, M. Coelho, A.E. Rodrigues, Microencapsulation of essential oils with biodegradable polymeric carriers for cosmetic applications, Chem. Eng. J. 245 (2014) 191–200.

[45] D. Zhang, A.B. Karki, D. Rutman, D.P. Young, A. Wang, D. Cocke, T.H. Ho, Z. Guo, Electrospun polyacrylonitrile nanocomposite fibers reinforced with Fe3O4 nanoparticles: fabrication and property analysis, Polymer 50 (17) (2009) 4189–4198.

[46] Y. Yao, H. Liu, X. Ding, X. Jing, X. Gong, G. Zhou, Y. Fan, Preparation and characterization of silk fibroin/poly(l-lactide-co-ε-caprolactone) nanofibrous membranes for tissue engineering applications, J. Bioact. Compat Polym. 30 (6) (2015) 633–648.

[47] F.J. Alenghat, D.E. Ingber, Mechanotransduction: all signals point to cytoskeleton, matrix, and integrins, Sci. STKE 119 (2002) pe6, 2002.

[48] D.J. Tobin, Introduction to skin aging, J. Tissue Viability 26 (1) (2017) 37–46.

[49] A. Arinstein, M. Burman, O. Gendelman, E. Zussman, Effect of supramolecular structure on polymer nanofibre elasticity, Nat. Nanotechnol. 2 (1) (2007) 59–62.

[50] P.J. Buch, Y. Chai, E.D. Goluch, Treating polymicrobial infections in chronic diabetic wounds, Clin. Microbiol. Rev. 32 (2) (2019) e00091-18.

[51] I. Chow, E.V. Lemos, T.R. Einarson, Management and prevention of diabetic foot ulcers and infections, Pharmacoeconomics 26 (12) (2008) 1019–1035.

[52] M. Fazli, T. Bjarnsholt, K. Kirketerp-Møller, B. Jørgensen, A.S. Andersen, K. A. Krogfelt, M. Givskov, T. Tolker-Nielsen, Nonrandom distribution of Pseudomonas aeruginosa and Staphylococcus aureus in chronic wounds, J. Clin. Microbiol. 47 (12) (2009) 4084–4089.

[53] M. Anvarinejad, G. Pouladfar, A. Japoni, S. Bolandparvaz, Z. Satiary, P. Abbasi, J. Mardaneh, Isolation and antibiotic susceptibility of the microorganisms isolated from diabetic foot infections in Nemazee Hospital, Southern Iran, J. Pathog. 2015 (2015).

[54] M. Sienkiewicz, M. Wasiela, A. Głowacka, [The antibacterial activity of oregano essential oil (Origanum heracleoticum L.) against clinical strains of Escherichia coli and Pseudomonas aeruginosa], Med. Dosw. Mikrobiol. 64 (4) (2012) 297–307.

[55] S.G. Ali, M.A. Ansari, M.A. Alzohairy, M.N. Alomary, M. Jalal, S. AlYahya, S.M. M. Asiri, H.M. Khan, Effect of biosynthesized ZnO nanoparticles on multi-drug resistant Pseudomonas aeruginosa, Antibiotics 9 (5) (2020) 260.

[56] R. Lambert, P.N. Skandamis, P.J. Coote, G.J. Nychas, A study of the minimum inhibitory concentration and mode of action of oregano essential oil, thymol and carvacrol, J. Appl. Microbiol. 91 (3) (2001) 453–462.
[57] S. Scandorieiro, L.C. de Camargo, C.A. Lancheros, S.F. Yamada-Ogatta, C. V. Nakamura, A.G. de Oliveira, C.G. Andrade, N. Duran, G. Nakazato, R. K. Kobayashi, Synergistic and additive effect of oregano essential oil and biological silver nanoparticles against multidrug-resistant bacterial strains, Front. Microbiol. 7 (2016) 760.
[58] S. Scandorieiro, L.C. de Camargo, C.A. Lancheros, S.F. Yamada-Ogatta, C. V. Nakamura, A.G. de Oliveira, C.G. Andrade, N. Duran, G. Nakazato, R. K. Kobayashi, Synergistic and additive effect of oregano essential oil and biological silver nanoparticles against multidrug-resistant bacterial strains, Front. Microbiol. 7 (2016) 760.
[59] G. Windiasti, J. Feng, L. Ma, Y. Hu, M.J. Hakeem, K. Amoako, P. Delaquis, X. Lu, Investigating the synergistic antimicrobial effect of carvacrol and zinc oxide nanoparticles against Campylobacter jejuni, Food Contr. 96 (2019) 39–46.
[60] M. Cristani, M. D'Arrigo, G. Mandalari, F. Castelli, M.G. Sarpietro, D. Micieli, V. Venuti, G. Bisignano, A. Saija, D. Trombetta, Interaction of four monoterpenes contained in essential oils with model membranes: implications for their antibacterial activity, J. Agric. Food Chem. 55 (15) (2007) 6300–6308.
[61] V. Tiwari, N. Mishra, K. Gadani, P.S. Solanki, N.A. Shah, M. Tiwari, Mechanism of anti-bacterial activity of zinc oxide nanoparticle against carbapenem-resistant acinetobacter baumannii, Front. Microbiol. 9 (1218) (2018).
[62] A. Nouvong, A.M. Ambrus, E.R. Zhang, L. Hultman, H.A. Coller, Reactive oxygen species and bacterial biofilms in diabetic wound healing, Physiol. Genom. 48 (12) (2016) 889–896.
[63] S.S. Lee, W. Song, M. Cho, H.L. Puppala, P. Nguyen, H. Zhu, L. Segatori, V. L. Colvin, Antioxidant properties of cerium oxide nanocrystals as a function of nanocrystal diameter and surface coating, ACS Nano 7 (11) (2013) 9693–9703.
[64] I. Rodriguez-Garcia, B.A. Silva-Espinoza, L.A. Ortega-Ramirez, J.M. Leyva, M. W. Siddiqui, M.R. Cruz-Valenzuela, G.A. Gonzalez-Aguilar, J.F. Ayala-Zavala, Oregano essential oil as an antimicrobial and antioxidant additive in food products, Crit. Rev. Food Sci. Nutr. 56 (10) (2016) 1717–1727.
[65] S. Hackenberg, A. Scherzed, A. Technau, M. Kessler, K. Froelich, C. Ginzkey, C. Koehler, M. Burghartz, R. Hagen, N. Kleinsasser, Cytotoxic, genotoxic and pro-inflammatory effects of zinc oxide nanoparticles in human nasal mucosa cells in vitro, Toxicol. Vitro 25 (3) (2011) 657–663.
[66] M. Saber, R.-S. Hayaei-Tehrani, S. Mokhtari, P. Hoorzad, F. Esfandiari, In vitro cytotoxicity of zinc oxide nanoparticles in mouse ovarian germ cells, Toxicol. Vitro 70 (2021), 105032.
[67] R. Augustine, H.N. Malik, D.K. Singhal, A. Mukherjee, D. Malakar, N. Kalarikkal, S. Thomas, Electrospun polycaprolactone/ZnO nanocomposite membranes as biomaterials with antibacterial and cell adhesion properties, J. Polym. Res. 21 (3) (2014) 347.
[68] S. Frank, G. Hübner, G. Breier, M.T. Longaker, D.G. Greenhalgh, S. Werner, Regulation of vascular endothelial growth factor expression in cultured keratinocytes. Implications for normal and impaired wound healing, J. Biol. Chem. 270 (21) (1995) 12607–12613.
[69] J. Xu, C. Zgheib, M.M. Hodges, R.C. Caskey, J. Hu, K.W. Liechty, Mesenchymal stem cells correct impaired diabetic wound healing by decreasing ECM proteolysis, Physiol. Genom. 49 (10) (2017) 541–548.
[70] H. Li, J. Chang, Bioactive silicate materials stimulate angiogenesis in fibroblast and endothelial cell co-culture system through paracrine effect, Acta Biomater. 9 (6) (2013) 6981–6991.
[71] H. Bai, N. Kyu-Cheol, Z. Wang, Y. Cui, H. Liu, H. Liu, Y. Feng, Y. Zhao, Q. Lin, Z. Li, Regulation of inflammatory microenvironment using a self-healing hydrogel loaded with BM-MSCs for advanced wound healing in rat diabetic foot ulcers, J. Tissue Eng. 11 (2020), 2041731420947242.
[72] R.E. Mirza, T.J. Koh, Contributions of cell subsets to cytokine production during normal and impaired wound healing, Cytokine 71 (2) (2015) 409–412.
[73] I. Christiaens, D.B. Zaragoza, L. Guilbert, S.A. Robertson, B.F. Mitchell, D.M. Olson, Inflammatory processes in preterm and term parturition, J. Reprod. Immunol. 79 (1) (2008) 50–57.
[74] S. Patel, S. Srivastava, M.R. Singh, D. Singh, Mechanistic insight into diabetic wounds: pathogenesis, molecular targets and treatment strategies to pace wound healing, Biomed. Pharmacother. 112 (2019) 108615.
[75] R. Gary Sibbald, K.Y. Woo, The biology of chronic foot ulcers in persons with diabetes, Diabetes Metab. Res. Rev. 24 (Suppl 1) (2008) S25–30.

**Dr. Xiumei Mo**: Dr. Xiumei Mo is affiliated to College of Chemistry, Chemical Engineering and Biotechnology, Donghua University, where She is currently working as Professor. She has authored and co-authored several national and international publications and also working as a reviewer for reputed professional journals. She is having an active association with different societies and academies around the world. She made his mark in the scientific community with the contributions and widely recognition from honourable subject experts around the world. Her major research interest involves in fabricating regenerative biomaterial and polymer-based controlled drug delivery systems.

**Atta ur Rehman Khan**: Atta ur Rehman Khan is a doctoral fellow at Donghua University. His core interests include the fabrication of polymer-based drug delivery system mainly through electrospinning and 3D printing techniques. His major interest is to achieve functionality in polymers by loading natural bioactive compounds. His major focus is to use alternate antibacterial agents to combat the problem of bacterial resistance against conventional antibacterial agents. His doctoral project is fabrication, physicochemical characterization and biological evaluation of electrospun nanofibers for the treatment of diabetic foot ulcer.